MINISTRY OF EDUCATION AND RESEARCH
POLITEHNICA University of Bucharest
Doctoral School of
Industrial Engineering and Robotics

Alexandru Gh. Paraschiv

PhD THESIS SUMMARY

Research on the development of innovative manufacturing technologies for increasing the performance of complex gasodynamic components

***PhD Supervision*,**
Prof.Dr.Eng. Cristian Doicin

- 2021 -

POLITEHNICA University of Bucharest

CSUD UPB decision no. 473 from 01.11.2019

Alexandru Gh. Paraschiv

PhD THESIS SUMMARY

Research on the development of innovative manufacturing technologies for increasing the performance of complex gasodynamic components

PhD Evaluation Board

President	Prof.dr.eng. Marian GHEORGHE	POLITEHNICA University of Bucharest
PhD supervisor	Prof.dr.eng. Cristian Vasile DOICIN	
Referent	Prof.dr.eng. Gheorghe OANCEA	TRANSILVANIA University of Brașov
Referent	Prof.dr.eng. Nicolae BÂLC	Technical University of Cluj-Napoca
Referent	Prof.dr.eng. Alexandra BANU	POLITEHNICA University of Bucharest

- 2021 -

Content

Introduction

The current requirements for the development of high-efficiency, low-impact gas turbines are still challenging to achieve, regardless of their application in the power, aviation or marine industries. One solution unanimously accepted by the engineering community *(***National Aeronautics and Space Administration 2020, ***Community Research and Development Information Service 2008*) to improve energy efficiency and reduce NOx and CO2 emissions from gas turbines is to increase the turbine's operating temperatures and gas pressure. However, in modern turbine engines, the Turbine Entry Temperatures (TET) exceed the melting point of even the most advanced superalloys of which the parts from the hot zone of the gas turbine engines (complex gasodynamic components) are made. Therefore, these components' optimum operation depends on advanced cooling systems and special heat-protected alloys with surface coatings with high resistance to oxidation and corrosion at high temperatures.

In turbine blades, the new design concepts involve increasingly complex geometries and internal cooling channels, with thin walls that exceed the practical possibilities of conventional manufacturing technologies, by precision casting. One solution that the scientific community (****ETN Additive Manufacturing Working Group 2019, ***SIEMENS Gas Turbine Blades 2018)* and large international concerns (GE, Siemens) has emphasised in recent years is the use of additive manufacturing technologies based on the powder bed fusion (PBF) process, especially selective laser melting technology (SLM).

The SLM technology and, in general, the powder bed fusion (PBF) additive manufacturing (AM) processes with metallic powder had an impressive technological boost in recent years. Nevertheless, SLM technology still has several limitations related to optimising the process parameters, anisotropy of mechanical properties of additively manufactured material, reduction/elimination of post-processing operations and typical defects in additively manufactured parts. These are some of the topics that are extensively covered in this PhD thesis.

Once these challenges are overcome, the development of innovative Thermal Barrier Coatings (TBC) and improved thermal spray coating technology to increase the thermal capability and service life of additively manufactured components are the next steps in the long process of sustainable aerospace and energy development. Although the complementary use of additive manufacturing and thermal spraying technologies to manufacture complex gasodynamic components is still a subject not thoroughly explored worldwide, this PhD thesis deals comprehensively with this topic in relation to conventional manufacturing technologies.

Based on these considerations, the research aimed at developing and characterising an advanced system for thermal protection of turbine blades, consisting of a substrate, obtained through additive manufacturing by selective laser melting, protected with a thermal barrier coating deposited by thermal spraying, hereafter called substrate/TBC coating system.

Part I, consisting of two chapters, presents a critical review of the current state of research on additive manufacturing technology, focusing on SLM manufacturing processes and thermal spray technology. Based on this analysis, several experimental designs of substrate/TBC coating systems

have been proposed for development. A case study is also presented to determine the impact of increasing operating temperatures on the overall performance of a turbo engine.

Part I concludes with the third chapter, where the main conclusions from the literature analysis and the case study are presented.

The research and development directions were outlined based on the conclusions drawn from the state-of-the-art analysis of additive manufacturing and thermal spraying technologies. The main objective and research and development methodology of the PhD thesis were established, as presented in chapter four. Based on these aims, fundamental and applied research of considerable importance for developing additive manufacturing and thermal spraying technologies has been carried out, as presented in the second part of the PhD thesis.

The fifth chapter presents the contributions made by the author in terms of optimising the process parameters of SLM technology and analysing the impact of the orientation of the part on the manufacturing platform on the anisotropy of mechanical properties, the purpose being to manufacture an IN 625 alloy with mechanical performance close to 625 obtained by conventional technologies. The process parameters identified as optimal based on mechanical tests and microstructural investigations were used to manufacture an experimental turbine blade demonstrator with internal cooling channels. Orientation of the turbine blade on the manufacturing platform was chosen so that the supporting structures do not affect the pallet aerofoil and internal cooling ducts and do not require significant post-processing operations.

The sixth chapter contains contributions on numerical simulation modelling of the temperature distribution and internal stresses in experimental models of substrate/ TBC coating systems obtained from simulating the operating conditions of a military aircraft turboshaft engine. To validate the results obtained following the numerical simulation were produced support samples of laminated IN 625 alloy and additively fabricated IN 625 alloy and were thermal spray-coated with TBC coatings of various compositions, characteristics and architectures.

The seventh chapter presents theoretical and experimental contributions on cyclic oxidation testing at elevated temperatures and the characterisation of substrate/TBC coating systems. Both standardised methods and original methodologies were used to characterise the systems. The experimental data obtained were used for in-depth analyses aimed at the mechanical behaviour of substrate/TBC coating systems, the evolution of metallic bond coat surface roughness, the thickness of the thermally grown oxide layer and the porosity of the ceramic layer and the kinetics of the oxidation process of the coatings. In addition, the substrate/TBC coating systems were tested at different thermal shock cycles using an automated installation designed and developed during the PhD thesis. Finally, the best performing TBC coating and the associated deposition technology were used to coat the experimental turbine blade demonstrator fabricated by SLM technology.

The final chapter, chapter eight, summarises the overall conclusions of the thesis, the author's contributions and future research directions. The originality of the results obtained in the two areas of interest of this PhD thesis, additive manufacturing and thermal spraying, is supported by an invention patent granted by OSIM, the presentation of seven papers in international conferences at the national and international level and the publication of 24 articles as first author and co-author in peer-reviewed journals.

On the occasion of the finalisation of doctoral studies, I would like to thank my PhD coordinator, Prof. Dr. Eng. Cristian Doicin, Dean of the Faculty of Industrial Engineering and Robotics, of the University "POLITEHNICA" in Bucharest, both for the guidance received during the bachelor and master studies and for the support given in the elaboration and correction of the doctoral thesis.

I would also like to thank Prof. Dr. Eng. Alexandra Banu who helped to open my path to research and supported me in writing my PhD thesis.

Thanks to my colleagues in the Department of Special Components. Physical and Mechanical Testing Laboratory of the INCD Turbomotoare COMOTI, who encouraged me during the elaboration of my thesis and managed to implement several extravagant ideas materialised in numerous scientific papers.

Last but not least, I would like to thank my family and close people who supported and encouraged me throughout my doctoral studies.

The experimental research presented in the PhD thesis related to the technology and system of thermo-resistant coatings was financially supported under the project POC 114/09.09.2016, Project ID P_40_422, cod SMIS: 105884, with the title "*Developing innovative solutions for new products and technologies demanded by the market by leveraging expertise in advanced materials and transferring knowledge to the private sector*", acronym TRANSCUMAT, Project co-financed by the European Regional Development Fund through the Competitiveness Operational Program 2014-2020, Action 1.2.3. Partnerships for knowledge transfer. During the subsidiary contract no. 5/D.1.3/114/18.12.2017, within POC 114/2016, a contract concluded between INCD Turbomotoare COMOTI and SC PLASMA JET SRL a new product, "New technology and system for heat-resistant coatings", has been developed, representing the pre-determined indicator of achievement: "Number of companies benefiting from new product market introduction support - CO28".

The experimental research presented in the PhD thesis related to the additive manufacturing technology was financially supported under contract 7N/2018, entitled "*Theoretical and experimental research on the response mechanisms of anisotropic materials to thermal and/or mechanical stresses*", of the Nucleu programme 2019-2020 funded by the Ministry of Research and Innovation (programme name "Theoretical and experimental research to increase the performance of air and ground propulsion systems in 2018", acronym Turbo 2020+).

Alexandru Paraschiv

Glossary of Terms

Nr. Crt.	***Abrev.***	***Significance***
01	ASTM	American Society for Testing and Materials
02	AM	Additive Manufacturing
03	APS	Atmospheric Plasma Spraying
04	CAD	Computer-Aided Design
05	DED	Direct Energy Deposition
06	DMLS	Direct Metal Laser sintering
07	EBM	Electron Beam Melting
08	EB-PVD	Electron Beam Physical Vapor Deposition
09	EDS	Energy-Dispersive X-ray Spectroscopy
10	GZO	Gadolinium Zirconium Oxide
11	HIP	Hot isostatic pressing
12	HVOF	High Velocity Oxygen Fuel
13	IN 625	Nickel-based superalloy Inconel 625
14	LZO	Lanthanum Zirconium Oxide
15	PBF	Powder Bed Fusion
16	SEM	Scanning Electron Microscope
17	SLM	Selective Laser Melting
18	STL	Standard Tessellation Language
19	TBC	Thermal Barrier Coatings
21	TET	Turbine Entry Temperature
22	TGO	Thermally Grown Oxide
23	TIF	Tagged Image File
24	TRL	Technology Readiness Level
25	YSZ	Yttria-Stabilized Zirconia

Chapter 1. Current status of research on additive manufacturing of complex gasodynamic components

1.1 Additive manufacturing technology

Additive manufacturing (AM), also known as" 3D printing"," additive production"," additive process" or "free manufacture", is defined as "The process of joining materials to form objects from a 3D CAD model, usually layer by layer, as opposed to subtractive and formative manufacturing technologies". Additive manufacturing processes are divided into seven categories: Vat photopolymerisation, Material extrusion, Material jetting, Binder jetting, Powder bed fusion, Directed energy deposition, Sheet lamination (****Standard ISO/ASTM DIS 52900 2018, Ulmeanu M. și Doicin C. 2018*).

1.2 Additive manufacturing by powder bed fusion

Depending on how the raw material is melted and the type of energy source generated for the fusion of particle, the leading additive manufacturing technologies using the Powder Bed Fusion (PBF) process are Selective Laser Melting (SLM), Direct Metal Laser Sintering (DMLS), Electron Beam Melting (EBM), Selective Heat Sintering (SHS) and Selective Laser Sintering (SLS).

Comparative analysis of the advantages and disadvantages of PBF type manufacturing technologies revealed that additive manufacturing using SLM technology is a promising alternative to conventional manufacturing technologies for the manufacturing of complex gasodynamic components due to design freedom, high mechanical properties of the manufactured parts, simplified production steps and reduced (****González D. S. și Álvarez A. G. 2018*, ****ETN Additive Manufacturing Working Group 2019*).

1.3 SLM technology

SLM is the additive manufacturing technology in which a laser beam selectively and in a controlled manner melts successive layers of powder (from a metal powder bed) depending on the cross-sectional geometry of the digital pattern being processed and the process parameters set (Fig. 1.1).

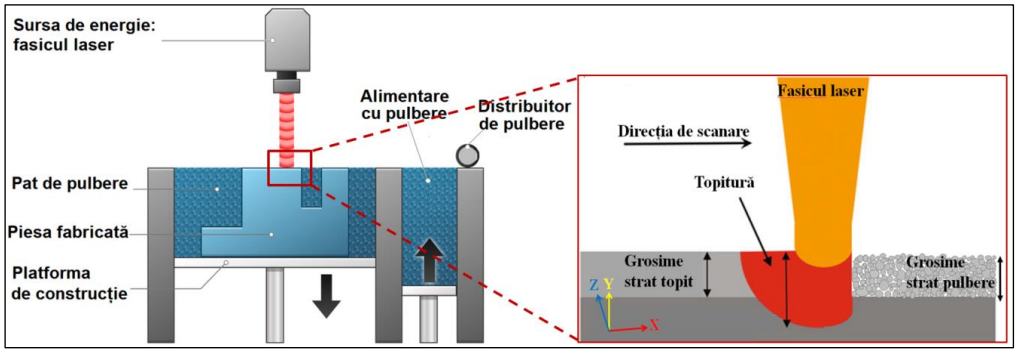

Fig. 1.1 *Powder bed fusion process by selective laser melting (SLM) (adapted from ***Dassault Systemes 2018, Milewski J.O. 2017)*

The technology (SLM) has several limitations related to low surface quality, anisotropy of mechanical properties, material defects, the need for support structures and pre- and post-processing operations of manufactured parts (*Han P. 2017*). The main challenges for SLM technology are: obtaining high-density materials (close to 100%), maximisation of mechanical properties, improving surface quality, reducing internal stresses in the material, increasing productivity, developing testing and validation procedures for additively manufactured parts and ensuring good repeatability of the manufacturing. (*Kruth J.-P. et al. 2010*, *Brandt M. 2016*, *Leary M. 2017*). Numerous factors influence the characteristics and properties of the products manufactured additive by SLM technology represented schematically in Fig. 1.2.

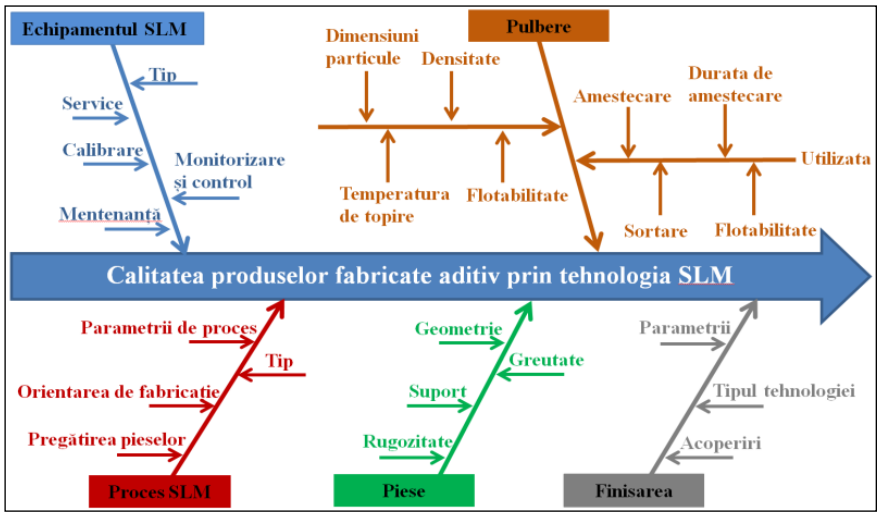

Fig. 1.2 *The factors that influence the quality of a product obtained by SLM technology (adapted from Khaimovich A.I et al. 2019)*

The most critical process parameters that affect the surface quality and mechanical properties of selective laser melted (SLMed) parts are laser power and speed, melt thickness, scanning strategy and the part orientation on the manufacturing platform (*Hanzl et al. 2015*, *Kempen K. et al. 2011*, *Ban A. M. și Aboutaleb L. 2018*, *Sufiiarov et al. 2017*, *Khoda B. 2017*). The optimisation of the process parameters is carried out on assessing the effects on the properties and characteristics of the additively manufactured alloy, and the variation should be carried out independently and not in combination.

1.4 Additive manufacturing of complex gasodynamic components

The most important advantages of additive manufacturing are the possibilities to design parts without restrictions (freedom of design) and to manufacture in a shorter time, with less energy and raw material consumption than conventional technologies, making it particularly attractive for manufacturing parts where geometries are very difficult or impossible to achieve with conventional technologies.

To manufacture the metal components in a gas turbine engine, the components that involve high manufacturing costs and times using conventional technologies are targeted, such as rotating critical components (compressor blades, compressor rotor assembly, turbine blades and turbine discs) (****Siemens 3D Printed Gas Turbine Blades 2016*, ****TURBOCAM International 2018*, *Magerramova*

L. et al. 2018) and static (burners, nozzles and fuel injectors) (*Petrat T. et al. 2016*, *Liu R. et al. 2017*, *F. Pankotai și Rawlins F. 2018*).

1.5 Turbine blade manufacturing technologies

The manufacturing technologies used to produce turbine blades are considered high-performance technologies but very expensive and limited. In addition, in recent years, blade design concepts have required increasingly sophisticated geometries with thin walls and complex internal cooling channels that make it difficult or even impossible to manufacture blades by precision casting. In the case of technological casting and machining processes, material losses are incredibly high, in some cases even reaching 95% of the total material used. In contrast, in the additive manufacturing case, due to the possibility of reusing and recycling the powder used, losses are usually no more than 5%. (*Nickels L. 2015*). In addition, *Nickels L.* (*2015*) showed that using additive manufacturing, the cost and manufacturing time of a component for an aircraft application can be reduced by up to 75% compared to the same component made using conventional technologies. On the other hand, the dimensional and geometric tolerances imposed by aerospace applications are impossible to meet in the absence of processing and finishing the additive-manufactured parts' surfaces. Furthermore, the lack of results or high degree of spreading of experimental data makes the transition from conventional to additive manufacturing for manufacturing complex gasodynamic components to be carried out slowly and with several technological limitations.

SLM technology is a viable solution for manufacturing a turbine blade with improved operating performance. A representative example is a nickel-based superalloy turbine blade, additively manufactured and tested under actual operating conditions at the Siemens industrial concern. (****Siemens 3D Printed Gas Turbine Blades 2016*). Various research on the additive manufacturing of turbine blades using different materials and additive manufacturing technologies is reported in the literature. Turbine blades with different geometries and dimensions have been manufactured by DMLS technology (with IN 718) (*Caiazzo F. et al. 2017*), SLM technology (with IN 939 alloy) (*Shaikh A.S. 2018*) or by DED technology (with steel type SS316L) (*Wilson J. M. 2014*). Other studies aimed at adapting additive manufacturing processes to rebuild degraded turbine blades. *V. G. Smelov et al.* (*2016*) și *E. Salvati et al.* (*2017*) used additive manufacturing to rebuild compressor blades from SS316L using SLM technology and from IN 718 using DED technology, respectively. The research in these studies aimed to identify and prevent the defects that occur in additively manufactured blades, the most common being porosity, microcracks and, in isolation, defects such as lack of fusion, deformation, balling or the appearance of inclusions (*Caiazzo F. et al. 2017*).

The technological process of additive manufacturing of a turbine blade is carried out in three main stages. In the first stage, the 3D model of the turbine blade is designed based on the gas-dynamic requirements and the design for additive manufacturing. In the second stage (processing), the preparation of the equipment (fixing the manufacturing platform, adjusting the thickness of the powder layer distributed on the platform, setting the process parameters, etc.) and the actual manufacturing of the part are carried out. Finally, depending on the requirements of the manufactured part, various post-processing operations can be applied in the last stage of the manufacturing process: heat treatments, hot isostatic pressing (HIP), sandblasting, deposition of coatings, machining and/or electro-erosion, etc.) (****ETN Additive Manufacturing Working Group 2019*). The typical deposition technologies for TBC coatings for turbine blade protection are electron

beam physical vapour deposition and thermal spray deposition (*Bose S. și DeMasi-Marcin T. J. 1997*), the latter being the most suitable for depositing thick coatings with low thermal conductivity and high durability under advantageous (*Feuerstein A. et al.* (*2007*).

1.6 Impact of increasing the operating temperature of the complex gasodynamic components on overall gas turbine engine performance.

Using an effective TBC coating ensures an increase of up to 150°C (*Muktinutalapati N.R. 2011*) in the operating temperatures of the components it protects and, consequently, an improvement in the overall performance of the gas turbine engine. Using the F110-220E turbojet-engine thrust augmentation used in F16 and F15 military aircraft as a study model, the impact of a (hypothetical) 50°C increase (from 1200°C to 1250°C) in engine operating temperatures were analysed, resulting in a 4% increase in thrust and a 3% decrease in specific fuel consumption.

Chapter 2. Current status of research on the manufacture of thermal barrier coatings for the protection of complex gasodynamic components

2.1 Introduction

The operating temperatures in gas turbine engines far exceed the temperatures at which the superalloys of which the parts from the hot zone of the gas turbine engines are made can operate optimally. Thermal Barrier Coatings (TBC) is the only viable solution for increasing operating temperatures and protecting components against oxidation and corrosion. Fig. 2.1 shows the influence of a TBC coating on the temperature gradient in a fixed turbine blade schematically.

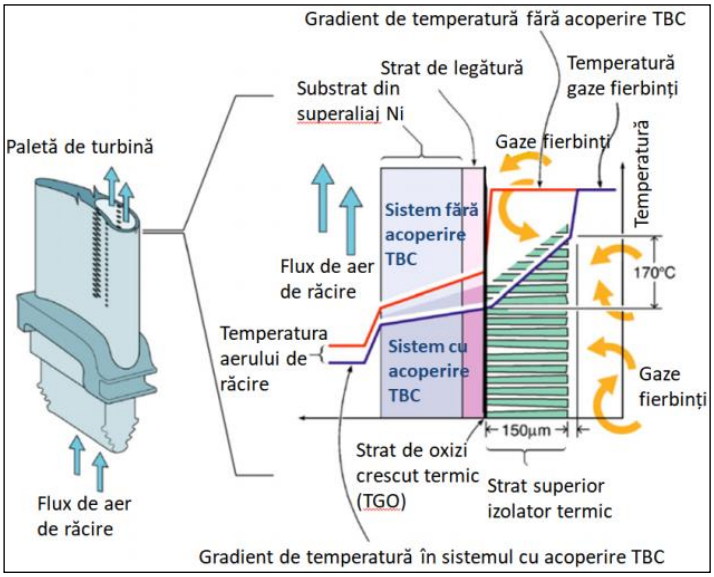

Fig. 2.1 *Temperature transition in a TBC coating deposited on a fixed turbine blade with internal cooling channels (adapted from Yu Z. et al. 2006)*

2.2 Structure of a substrate/ TBC coating system

A substrate/ TBC coating system (Fig. 2.2) is composed of a substrate (base material) and a TBC coating consisting of three layers: (i) a metallic Bond Coat; (ii) a ceramic Top Coat acting as a thermal barrier; (iii) a Thermally Grown Oxide (TGO) layer acting as a diffusion barrier against the propagation of oxygen from the air to the substrate.

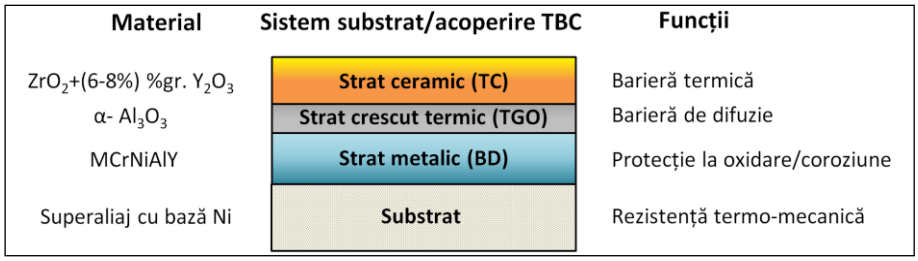

Fig. 2.2 Structure of a substrate/TBC coating system

2.3 Thermal spraying technology

Thermal spray deposition of material layers consists of heating, dispersion in a carrier gas jet and projection of the raw material (wires, rods, rods or powders) in the form of molten particles on the surface of support material (substrate) (*Fauchais P.L. et al. 2014*). The sprayed particles flatten and solidify as they hit the substrate or previously deposited layers, forming successive layers with thicknesses ranging from tens of microns to 5 mm.

Depending on the energy generated to melt the raw material, the thermal spraying technologies can be divided into three categories: (i) technologies using the energy generated by an electric arc, a plasma jet or an arc-transferred plasma; (ii) technologies using the energy generated by a combustion flame: thermal spraying by high-velocity oxygen fuel or detonation gun; (iii) technologies using the energy generated by compressed gases (cold spraying). Therefore, the performance of TBC coatings depends on a combination of factors shown schematically in Fig. 2.3.

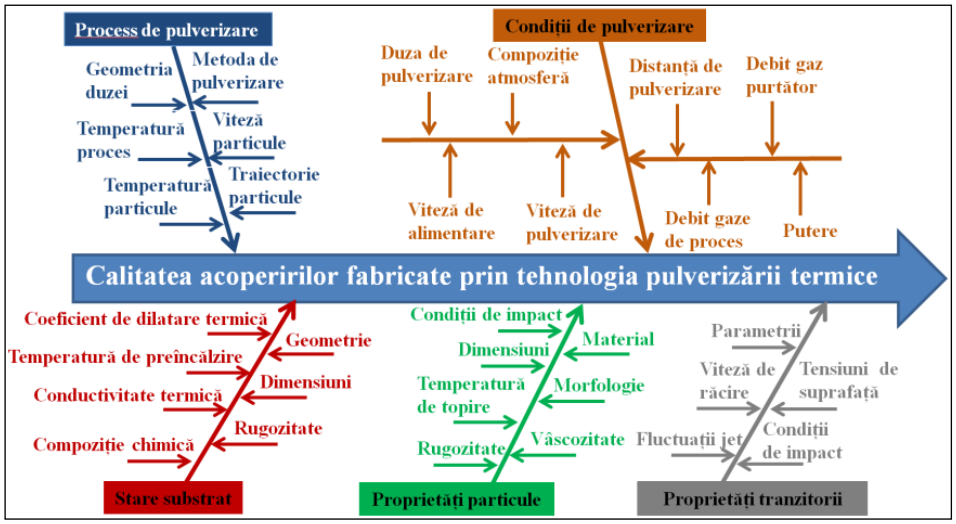

***Fig. 2.3** The factors that influence the quality of coatings deposited by thermal spray technology (adapted from Majumdar J. D. 2014, ***Science Learning Hub 2015)*

2.4 Oxidation behaviour at high temperatures

The components coated with TBC coatings in a gas turbine are affected during service by various types of degradation initiated mainly by the oxidation process at high temperatures. (*Evans A. G. et al. 2008*).

The oxidation kinetics at elevated temperatures can be determined by measuring the mass growth or thickness of the TGO oxide layer (*A. Banu, A. Paraschiv et al. 2020*) when the oxidation rate of a metal as a function of oxidation time will follow one of three mass growth laws: linear (Relation 2.1), logarithmic (Relation 2.2) or parabolic (Relation 2.3) (*Pimin Z. 2018*).

$$x = k_1 \cdot t \quad (2.1)$$

$$x = k_e \log (a \cdot t+1) \quad (2.2)$$

$$x^2 = kp \cdot t \quad (2.3)$$

Where: *ke/k* is the oxidation rate constant, *x* is the increase in mass (g) of the sample or thickness (m) of the oxide layer, *t* is the oxidation time (s), and a is a constant.

2.5. Limitations of conventional TBC coatings

The current performance of TBC coatings with 7-8% Y2O3 yttria-stabilised zirconia ceramic layer (conventional YSZ) is limited at temperatures up to 1200°C due to zirconia phase transformations and the sintering process, with a relatively short operating life compared to the components in a gas turbine engine.

2.6. Identification of advanced materials to increase the performance of TBC coatings

Over the last decades, there has been a constant concern to improve or replace the ceramic layer (YSZ) in conventional TBC coatings, materialised by numerous studies. To increase the thermal shock resistance of TBC coatings, *Jamali H. et al.* (*2012*), *Wu J. et al.* (*2010*), *Wang W.Q. et al.* (*2006*) recommended replacing the conventional YSZ layer (obtained from micrometric sized particles) with a YSZ layer obtained from agglomerations of nanometric sized particles (nanostructured YSZ). The literature review also highlighted the following categories of materials as possible alternatives for conventional YSZ layer: perovskites, pyrochlores, aluminas and clusters (*Li.R. și Zhang M. 2015, Kokini K. et al. 1996, Cao X.Q, et al. 2004a*). Particular attention is paid to the zirconium oxides with rare earth, i.e. lanthanum (La2Zr2O7) and gadolinium zirconate (Gd2Zr2O7) (*Mahade S. et al. 2016, Pan W. et al. 2012, Liu et al. 2007*).

2.7. Choosing materials and manufacturing technologies

Based on the analysis of the current state of research, several experimental models of TBC coatings with different configurations, materials and top layer thicknesses have been proposed for development: TBC coatings with 7-8% yttria-stabilised zirconia layer obtained from micrometric sized particles (conventional YSZ) or agglomerations of nanometric sized particles (nanostructured YSZ),
TBC coatings with one or more layers of lanthanum Zr oxide (LZO) and/or gadolinium Zr oxide (GZO), with and without nanostructured YSZ layer.

Atmospheric Plasma Spraying (APS) technology was chosen for the development of TBC coatings, and a nickel-based superalloy representative for the manufacture of gas turbine components, Inconel 625 (IN 625), obtained conventionally (rolling) and by additive manufacturing, was used as base material.

Chapter 3. Conclusions on the state of the art of research into the manufacture of complex gasodynamic components and thermal barrier coatings

From the analysis of the current state of research on additive manufacturing of complex gasodynamic components, the following conclusions were drawn:

- Selective laser melting (SLM) additive manufacturing is a promising alternative to conventional technologies for manufacturing complex gasodynamic components;
- The most critical parameters in an SLM process are laser power and speed, scanning strategy, layer thickness and building orientation of part on the manufacturing platform. One of the main challenges of SLM technology is to optimise the process parameters to maximise the mechanical properties and to improve the quality of additively manufactured parts;
- SLM technology is a promising alternative to conventional technologies for the cost-effective production of a turbine blade with internal cooling channels capable of exceeding the performance of a turbine blade manufactured by a forging or precision casting.
- Typical TBC coating deposition technologies for high-temperature protection of turbine blades are electron beam physical vapour deposition and thermal spray deposition. The latter is the most suitable for the cost-effective deposition of thick coatings with low thermal conductivity and high durability.
- The use of thermal barrier coatings significantly improves the thermal capability of complex gasodynamic components.

From the analysis of the current state of research on the manufacture of thermal barrier coatings, the following conclusions were drawn:

- A TBC coating consists of a metallic bond coat, a ceramic top coat and a thermally grown oxide layer (which is formed by oxidation of the bond coat) between the metallic bond coat and ceramic top coat;
- The performance of TBC coatings depends on a combination of factors: thermal spraying technology, spraying conditions and parameters, and material properties;
- The current performance of TBC coatings with yttria-stabilised zirconia ceramic layer (conventional YSZ) is limited at temperatures up to 1200°C due to phase transformations of zirconia and the sintering process;
- The most promising materials for replacing the YSZ ceramic layer in conventional TBC coatings are considered to be nanostructured YSZ (obtained from agglomerations of nanometric sized particles), lanthanum and gadolinium zirconate.

Chapter 4. Contributions to the directions, main objective and research and development methodology of the PhD thesis

4.1 Research and development directions

The state-of-the-art analysis of additive manufacturing and thermal spray technologies revealed that the development of complex gasodynamic components for energy and aerospace applications using innovative manufacturing technology is currently a hot topic for which the following R&D directions have been outlined:

- Improvement of the SLM technology by optimising the critical process parameters to maximise the mechanical performance and quality of additively manufactured IN 625 alloy parts;
- Development of an innovative TBC coating for high-temperature oxidation protection of complex gas turbine engine components in a gas turbine engine.

4.2 The main objective of the research and development activity

Based on the analysis of the current state-of-the-art in additive manufacturing and thermal spraying technologies as well as R&D directions, the main objective of the PhD thesis is:

Development of an innovative technology for manufacturing complex gasodynamic components blade-type in a gas turbine engine, combining the SLM additive manufacturing technology for substrate manufacturing with the APS thermal spray technology to deposition a thermal barrier coating.

4.3 Research and development methodology

To achieve the main objective the research was conducted in three main stages.

I. Optimisation of the critical parameters in the SLM manufacturing process and manufacturing of an experimental model of a turbine blade with cooling channels;
II. Development of experimental models of TBC coatings using thermal spray technology for turbine blade protection, using conventionally and additively manufactured IN 625 alloy as substrate;
III. Analysis of the high-temperature behaviour of experimental models of substrate/TBC coating systems by long term oxidation and thermal shock tests.

Chapter 5. Contributions to the optimisation of parameters in the manufacturing process by selective laser melting

5.1 Manufacturing and characterisation of additively manufactured IN 625 alloy

To achieve the objective of optimising the critical parameters of the SLM manufacturing process, the effects on the mechanical properties and microstructural characteristics of IN 625 alloy were analysed by changing the following parameters: laser beam exposure time, laser beam current intensity, layer thickness and building orientation of the part on the X-Y-Z axes of the manufacturing platform. According to the experimental manufacturing and testing plan, identifying the optimal manufacturing parameters was carried out according to the rule of varying each parameter on several levels (see Tab. 5.1) and keeping the others at constant values. The principal criteria were the mechanical strength of the material and the microstructural characteristics of the manufactured alloy.

Tab. 5.1 *Experimental manufacturing and testing plan for IN 625 alloy specimens*

Current intensity [mA]	Laser exposure time [µs]	Layer thickness [µm]	Building orientation
2000	**28~**	50	YZ
2000	**52~**	50	YZ
2000	**64~**	50	YZ
2000	**76~**	50	YZ
2000	**40#**	50	YZ
600~	40	50	YZ
800~	40	50	YZ
1000~	40	50	YZ
1200~	40	50	YZ
1400~	40	50	YZ
1600~	40	50	YZ
1800~	40	50	YZ
2200~	40	50	YZ
2000#	40	**75~**	YZ
2000	40	**100~**	YZ
2000	40	**25~**	YZ
2000	40	**50~**	YZ
2000	40	**50#**	**XZ~**
2000	40	50	**Z~**
2000	40	50	**45°~**

~varied parameter; #optimized parameter

The choice of secondary parameters in the SLM process (defocus distance, scanning strategy, distances between two melts and between two scanning lines, parameters of support structures, etc.) was based on recommendations from the manufacturer of the manufacturing equipment and the results obtained in several studies carried out on the same additively manufactured alloy (*Paraschiv A. et al. 2020a-b*, *Matache M., Paraschiv A. et al. 2020a-b*, *Condruz M.R. et al. 2020b-d*).

The mechanical tests and microstructural investigations were carried out on cylindrical specimens and prismatic specimens (in the as-built state) (Fig. 5.1.b-d) manufactured with Lasertec 30 SLM equipment (DMG Mori, Germany) (Fig. 5.1.a) from IN 625 powder (LPW Technology Ltd.).

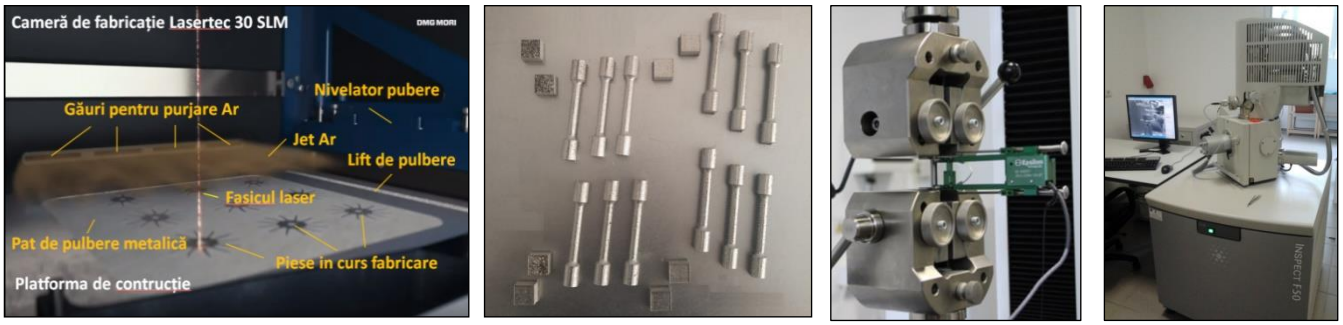

a) *b)* *c)* *d)*

Fig. 5.1 *SLM manufacturing and testing of IN 625 specimens: (a) 3D representation of the process chamber (adapted from***DMG MORI 2019); (b) fabrication of specimens on the construction platform, (c) tensile testing of specimens (Paraschiv A. et al. 2019a) and (d) microstructural characterisation of specimens*

The evaluation of the mechanical performance of IN 625 alloy was carried out by tensile tests at room temperature using a universal Dual Column Testing System INSTRON 3360 (Fig. 5.1. c) according to ISO 6892-1:2010. In addition, the microstructural investigations were performed using an FEI Inspect F50 field emission scanning electron microscope (SEM) equipped with an Apollo X SDD detector for Energy-Dispersive X-ray Spectroscopy (EDS) analysis of chemical elements and their distribution in the areas of interest.

5.2 Influence of changing process parameters on the microstructure and mechanical properties of additively manufactured IN 625 alloy

The main experimental results obtained after changing the process parameters on the mechanical properties and microstructural characteristics of IN 625 alloy are briefly presented below.

Laser exposure time. In Fig. 5.2.a-c are shown the average values (obtained based on three values) of the tensile strength (Rm), yield strength (Rp0.2), elongation (A5) and fracture toughness (Z) of IN 625 alloy specimens manufactured with the following exposure times: 28, 40, 52, 64 and 76 µs (see also Tab. 5.1).

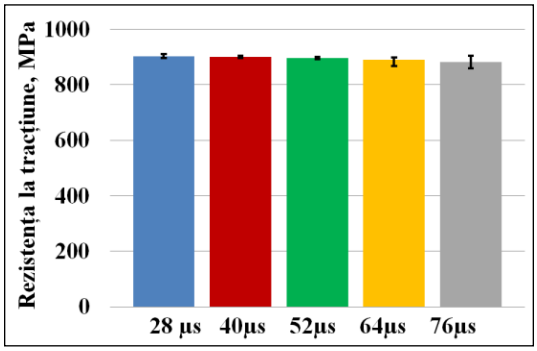

Fig. 5.2.a)

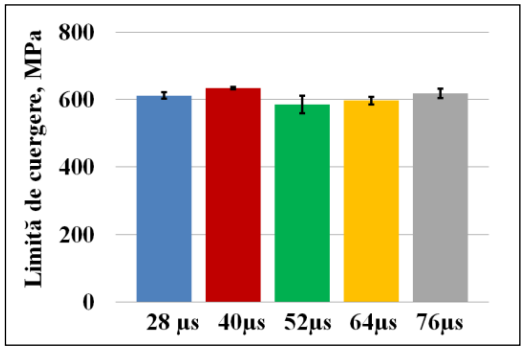

Fig. 5.2. b)

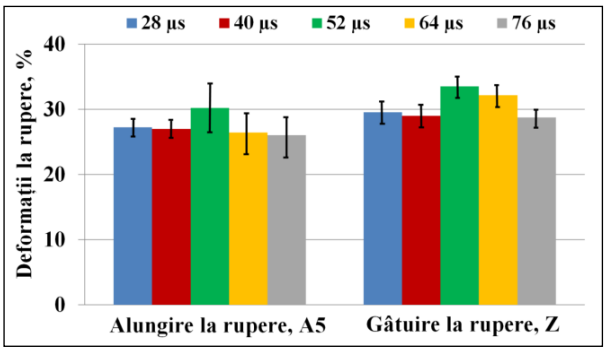

c)

Fig. 5.2 *Tensile test results of specimens manufactured with varying exposure times (adapted after Paraschiv A. et al. 2018b)*

The tensile test results showed that changing the laser exposure time does not significantly influence the mechanical strength of IN 625 alloy (see Fig. 5.2.a-c). Contradictory studies on the influence of scanning speed (laser exposure time) on the mechanical performance of some alloys manufactured by SLM technology have been identified in the literature. For example, *Zhang et al.* (*2011*) observed that the increasing scanning speed did not influence the tensile strength and yield strength of Ti2448 alloy, but the hardness and density of the material decreased. *Delgado J. et al. (2012)* and *Song et al.* (*2014*) have observed for several steels and Ni alloys that with increasing scanning speed, the mechanical performance of the materials decreases. The research was continued with microstructural investigations carried out on the as-built surfaces and subsequently on metallographically prepared surfaces of IN 625 samples. Fig. 5.3.a-d shows the SEM investigations performed on two manufactured samples with different exposure times (40 µs and 76 µs).

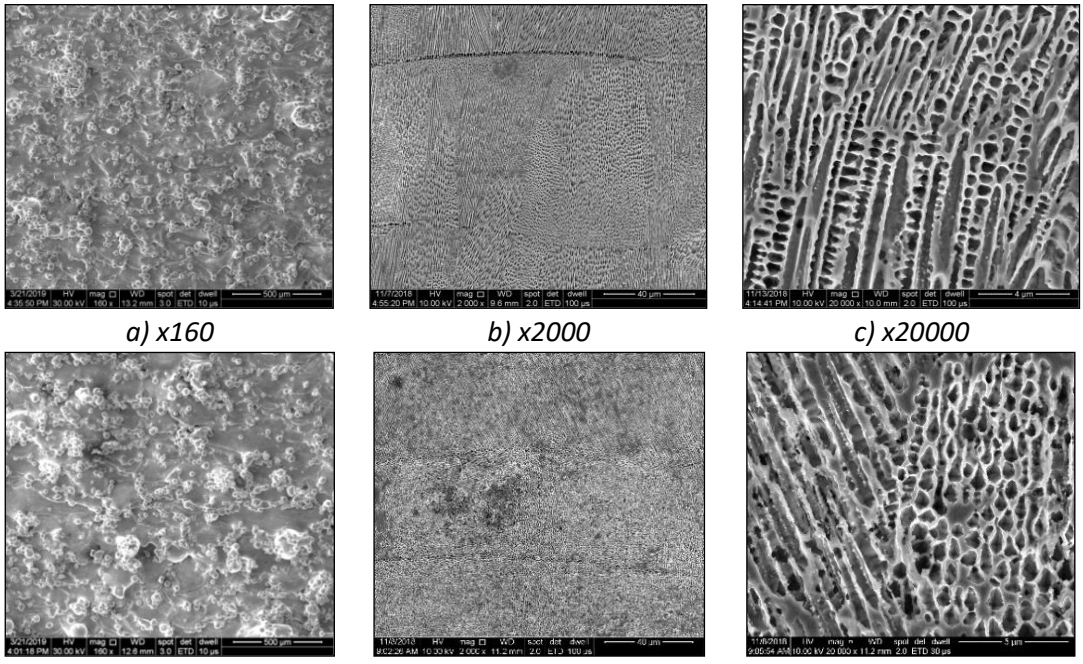

a) x160 *b) x2000* *c) x20000*

d) x160 *e) x2000* *f) x20000*

Fig. 5.3 *SEM images taken on the as-built (a,d) and metallographically prepared (b,c,e,f) surfaces of samples manufactured with different exposure times: (a-c) 40 µs and (d-f) 76 µs.*

SEM analysis performed on the as-built surface of the samples showed a reduction of the balling effect as the exposure times decreased below 52 µs. The analysis performed on the metallographically prepared surface of the samples revealed that the microstructure of the additively fabricated IN 625 alloy consists of dendritic structures oriented vertically to the next molten layer. By melting a new layer, the previous melt layer is partially re-melted, facilitating the growth of grains with the same crystallographic orientation through several layers. Increasing the exposure times, cooling and solidification of the molten material were slower, generating a coarser microstructure (see Fig. 5.3.f), affecting the material's mechanical performance during operation at elevated temperatures.

Based on the experimental results obtained from tensile tests, microstructural investigations and taking into account the productivity and manufacturing cost aspects, the optimal value of the **laser exposure time** parameter was considered to be 40 µs.

Similarly, the effects of changing current intensity and layer thickness were evaluated (see Tab. 5.1), and the main results and conclusions are summarised below:

- Changing the **current intensity** parameter had a high impact on the mechanical properties of IN 625 alloy. At a high value of intensity (2000 mA), the energy density generated by the laser beam allows the complete fusion of the particles, the partial re-melting of the previous molten layer and its welding to the new molten layer, resulting in the highest mechanical strength of the alloy (898±5 MPa). However, at low values of current intensity, the mechanical performance of the alloy decreases due to the occurrence of material defects such as lack of particle fusion, incomplete melting of the powder layer, pore formation and increased balling;
- **The layer thickness** is a parameter that influences both the mechanical strength of the alloy and the productivity of the manufacturing process. By increasing the thickness of the melt layer, the part's manufacturing time decreases, but the mechanical performance and the surface quality decrease (the "step" effect is accentuated). Analysis of tensile test results showed that a decrease below 50 µm of the layer thickness does not improve the mechanical properties, but using of thicknesses of 75-100 µm contributes to a significant decrease of the tensile strength and yield strength of IN 625;
- Analysis of the influence of changing process parameters on the mechanical properties and quality of additively manufactured IN 625 alloy revealed the following process parameters as optimal:

  - current intensity: 2000 mA;

  - laser exposure time: 40 µs;

  - layer thickness: 50 µm.

For anisotropy analysis of the mechanical properties of IN 625 alloy, sets of five specimens each were manufactured on X, Y, Z axes and rotated 45° in the XY plane of the fabrication platform using the optimal parameters determined in the previous step. The mechanical properties of the additively manufactured IN 625 specimens were compared with laminated IN 625 specimens (tested under similar conditions) and with the minimum values prescribed in ASTM F3056 and ASTM B 443 standards for nickel alloys obtained by PBF process and forging, respectively (see Fig. 5.4).

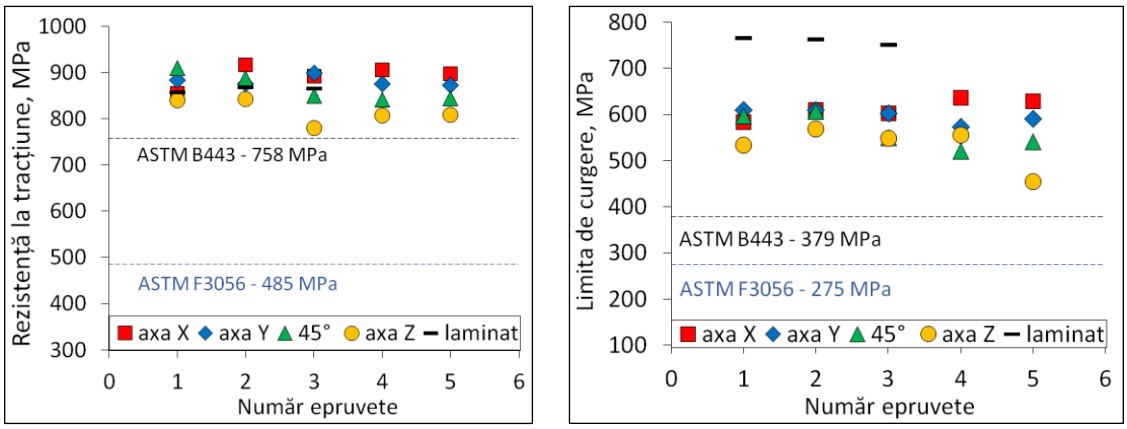

a) *b)*

Fig. 5.4 *Graphical representations of tensile properties of laminated and additively manufactured specimens on the X and Y axes, at 45° in the XY plane and on the Z-axis: (a) tensile strength and (b) yield strength*

The specimens manufactured in the horizontal plane had an average tensile strength (880 MPa) and yield strength (525 MPa) 6% and 8% higher, respectively, than the specimens manufactured in the vertical plane (Fig. 5.4). In addition, fractographic analysis of the specimen fracture surfaces (see Fig. 5.5.a-f) confirmed the anisotropy of the mechanical properties of IN 625 alloy. This behaviour was caused by the building orientation of specimens that influenced the orientation of the columnar grains (*Anam M.A. 2018*) and the cooling rates of the alloy during solidification (*Thijs et al. 2013*, *Liu et al. 2019*). The fracture of specimens made in the horizontal plane (X-axis) occurred both transcrystalline and intercrystalline, and the brittle aspect of fracture was determined by cleavage fracture, while the fracture of specimens made on the Z-axis was predominantly ductile (Fig. 5.5).

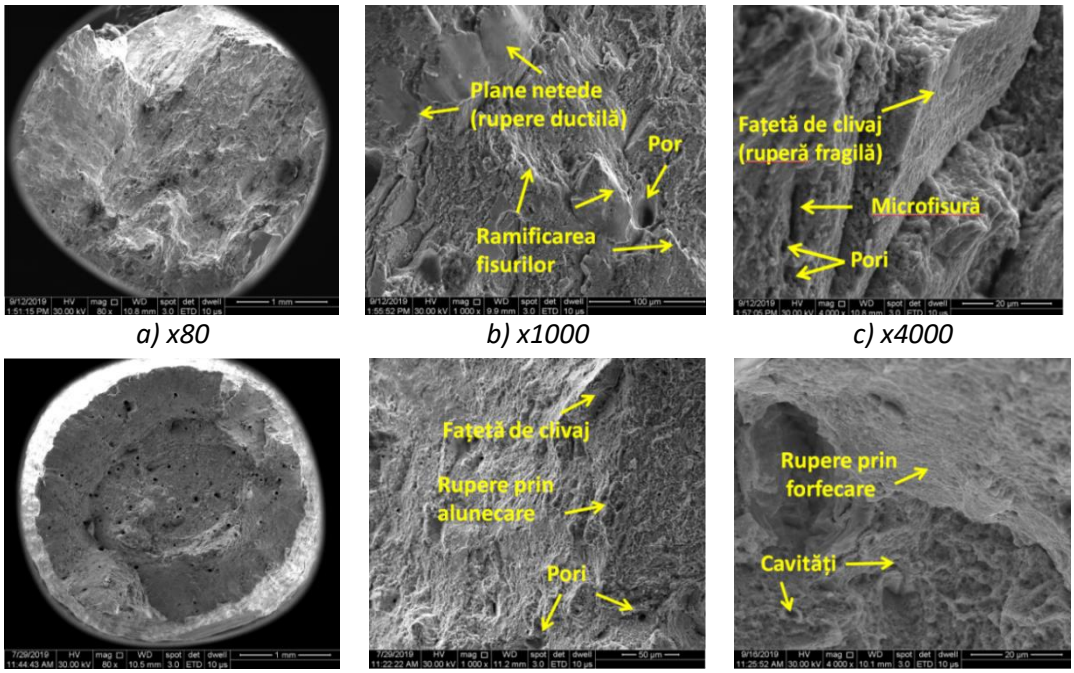

a) x80 *b) x1000* *c) x4000*

d) x80 *e) x1000* *f) x4000*

Fig. 5.5 *Fracture surface of additively manufactured specimens: (a-c) in the horizontal plane and (d-f) in the vertical plane*

The fracture surface of specimens manufactured in the vertical plane occurred by sliding and with large plastic deformations. As a result, the specimens acquired 65% and 25% more elongation and necking, respectively, than specimens manufactured in the horizontal plane of the manufacturing platform.

The experimental results showed that, regardless of the orientation of the specimens on the manufacturing platform (X, Y, Z axes and rotated at 45° in the XY plane), after optimisation of the process parameters, the IN 625 alloy was obtained with a fine microstructure, without defects or deformations and with a mechanical strength higher than the minimum values prescribed in the standards in force for this alloy, additively and conventionally manufactured (see also Fig. 5.4.a-b).

5.3 Manufacturing of the experimental turbine blade using SLM technology

A turbine blade model with internal cooling channels whose geometrical elements are oriented at angles less than 45° to the horizontal plane of the manufacturing platform was chosen for manufacturing the experimental turbine blade demonstrator. This geometry generally requires the use of support structures that may irreparably affect the aerofoil of the blade and the inner cooling channels of the blade (Fig. 5.6.a). Ansys 2020 R1 software (Additive Manufacturing module) was used to identify the blade's optimal building orientation. By entering the input data related to the minimum generation angle of the support structures, building orientation, optimisation after manufacturing time, level of internal stresses or volume of support structures, the optimal building orientation of the 3D CAD model (in terms of compliance with the requirements of a turbine blade) was determined after several iterations (Fig. 5.6.b). Using a dedicated program (RDesigner v2018) for setting the position of the part and the process parameters, the 3D model in *.stl* format was subjected to several iterations for the generation of support structures. Based on these iterations, the minimum angle of 28° (starting from 45°) between two surfaces for which the use of support structures is not necessarily required was identified (Fig. 5.6.c).

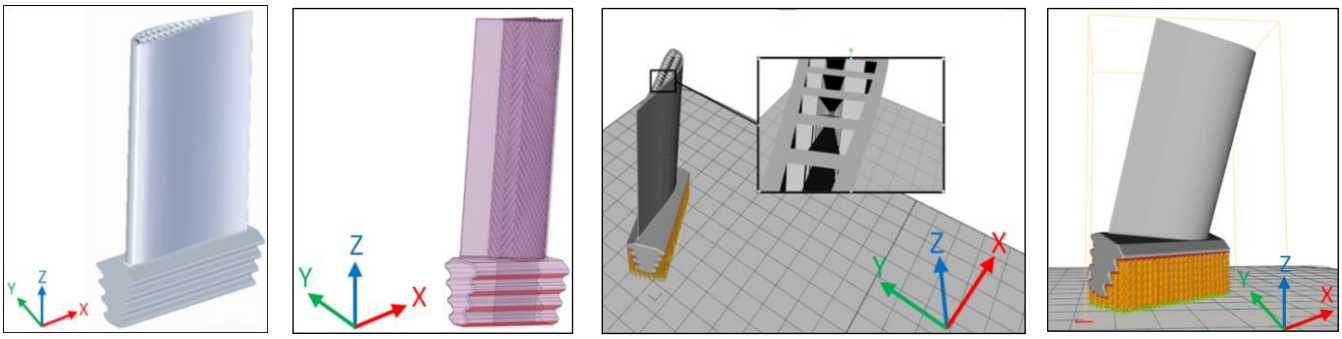

a) *b)* *c)* *d)*

Fig. 5.6 *Turbine blade orientation on the manufacturing platform: (a) 3D blade model, (b) identification of optimal blade orientation, (c) highlighting the missing support structures in the cooling channels, and (d) setting parameters and generating support structures*

Based on the chosen approach, no support structures were generated at the aerofoil level or inside the cooling channels, but only at the blade foot level (Fig. 5.6.d). However, at the blade foot, high-precision mechanical machining is subsequently required to respect the mounting dimensions of the blade in the rotor disc. After the generation of the support structures, process parameters

identified as optimal were set (see § 5.2), and the processed 3D model was introduced into the CELOS program of the Lasertec 30 SLM equipment. After the preliminary manufacturing operations (platform positioning, powder leveller adjustment, oxygen sensor calibration etc.) and the actual manufacturing (Fig. 5.7.a), the powder was vacuumed (Fig. 5.7.b), the support structures on the pallet leg (Fig. 5.7.c) were removed (Fig. 5.7.d), and the aerofoil surfaces to be thermally protected with TBC coatings were sandblasted (Fig. 5.7.e).

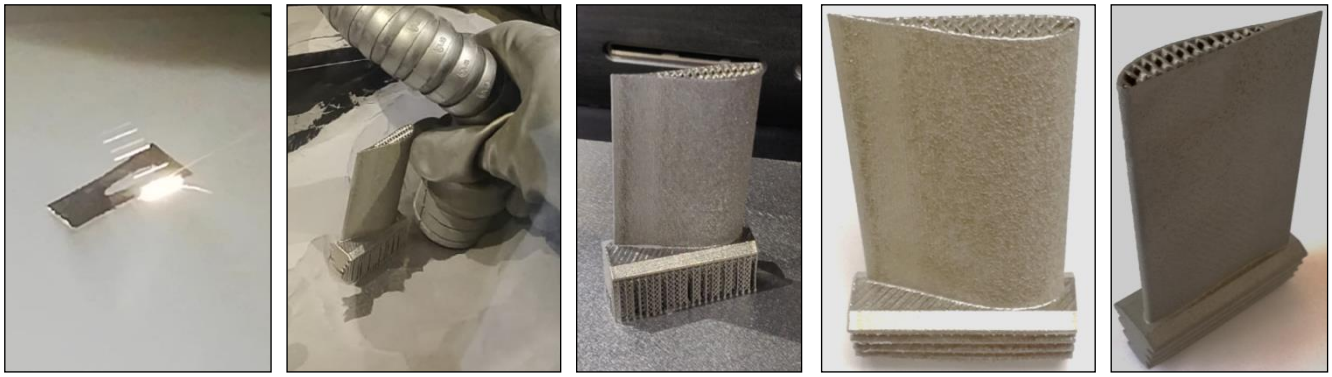

a) *b)* *c)* *(d)* *e)*

Fig. 5.7 *Additive manufacturing process by selective laser melting of the experimental blade model: (a) selective melting of layers (b) powder aspiration, (c) part cleaning (d) as-built blade and (e) sandblasted blade*

Concurrently with the research on the development of SLM technology for manufacturing the experimental turbine blade model, fundamental and applied research has been carried out on developing thermal barrier coatings (TBC) for thermal protection of turbine blades and other complex gas turbine components.

Chapter 6. Contributions to the numerical simulation modelling and manufacturing of the substrate/TBC coating systems

6.1 Numerical simulation modelling of the thermo-mechanical behaviour of the substrate/TBC coating systems at high temperatures

In the process of developing innovative TBC coatings, numerical simulation modelling of the high-temperature performance of the proposed substrate/TBC coating systems was performed (see § 2.7).

In the first part of the modelling process, the thermal conditions were imposed, and the results on the temperature distribution in the investigated systems were analysed. The imposing in the second part of the modelling process of a set of mechanical conditions was necessary to determine the internal stress state in the components of the systems.

The thermo-structural analysis was performed on six experimental models of substrate/TBC coating systems (E2T2-E2T7) and two reference models: a system without TBC coating (E2T0) and a system with a metallic coating (E2T1) (see Fig. 6.1).

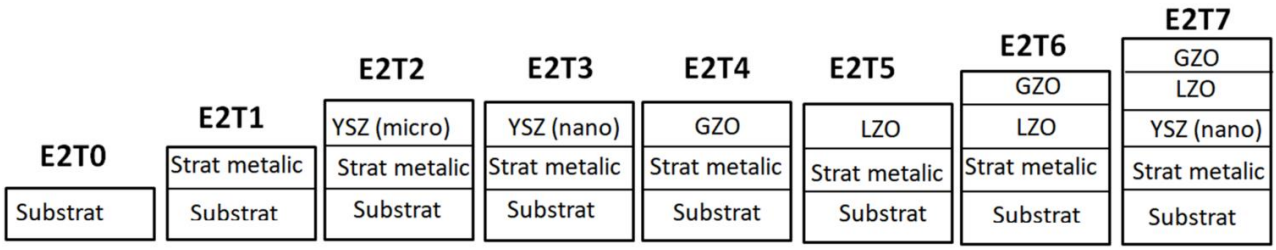

Fig. 6.1 *Experimental system models*

Using ANSYS R19.2 software, a reduced dimensional 3D model was produced for each variant of the substrate/TBC coating system to simplify the calculations. The 3D model was inserted into the working system where the network of nodes and elements (mesh) was created using the MultiZone method (Fig. 6.2.a-b). The embedding area of the models was set on the side surface of the models (Fig. 6.2.c) because, in actual conditions, the turbine blade with coatings is fixed at one end in the turbine disk.

Based on experimental data from the literature, the physical-mechanical properties (density and modulus of elasticity) and thermophysical properties (coefficient of thermal expansion, thermal conductivity and specific heat) of the materials were identified and introduced into the working system (*Feuerstein A. et al. 2007*, *Cao X. 2004b*, *Wang L. et al. 2014*).

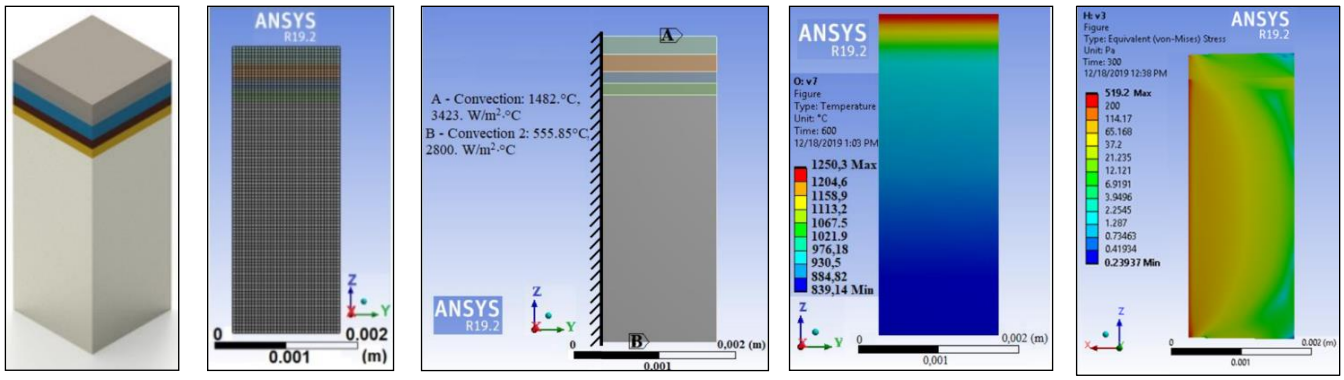

a) *b)* *c)* *d)* *e)*

Fig. 6.2 *Thermo-structural analysis of substrate/TBC coatings systems: (a-b) grid of points on the 3D model of the system; (c) convection zone setting and embedding zone representation, (d) temperature distribution and (e) von Mises stresses in the system (Frigioescu T. F., Paraschiv A. et al. 2020a)*

The thermal simulation consisted of heating the coated surface of the substrate/TBC coating systems with a high flow hot air jet and simultaneously cooling the opposite (uncoated) side with a cooler, lower flow air jet. The operating conditions of the F100-PW-220E engine turbine were chosen to simulate the temperature conditions at which a TBC substrate/coating system should operate. (Apostolidis A. 2015, Lee A. S. et al. 2009):

- Initial temperature: 22°C;
- Convection on the superior surface (coated): 3423 W/m^2°C, with a temperature of 1482°C;
- Convection on the inferior surface (uncoated): 2800 W/m^2°C, with a temperature of 556°C.

For a better overview of the simulation results, the data obtained in the substrate/metal substrate/ceramic substrate interfaces were processed using Octave software. In Fig. 6.3.a-b are

plotted for two systems (E2T3 and E2T7), the temperature drop values on the substrate, and in Fig. 6.3.c, the temperatures recorded at the substrate/coating interface of the analysed systems.

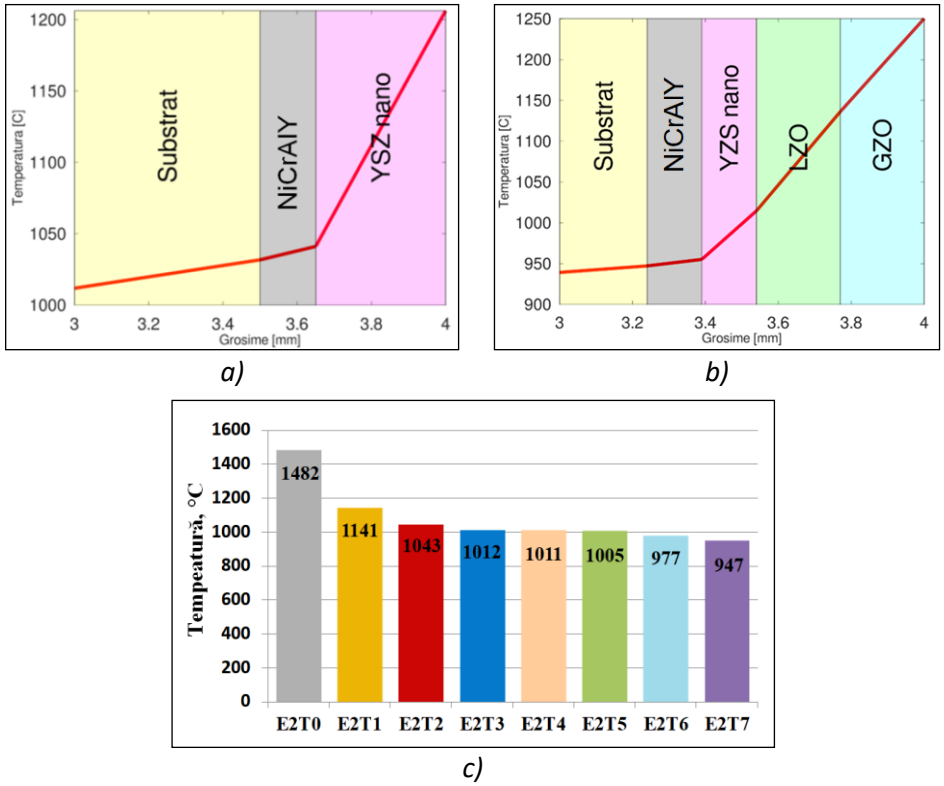

Fig. 6.3 *Determination of the temperature drop on the substrate: (a) in the E2T3 system, (b) in the E2T7 system, and (c) the temperatures at the substrate/TBC interface of the analysed systems (adapted from Frigioescu T. F., Paraschiv A. et al. 2020a)*

The thermo-structural simulation was performed for a two-time duration: 0.1 seconds to simulate thermal shock behaviour and after 300 seconds to simulate behaviour after temperature stabilisation. In Fig. 6.4.a-b, the von Mises stress distributions in two systems (E2T3 and E2T7) are plotted and in Tab. 6.1 the maximum values of the equivalent von Mises stresses recorded in the substrate/TBC systems after temperature stabilisation are centralised.

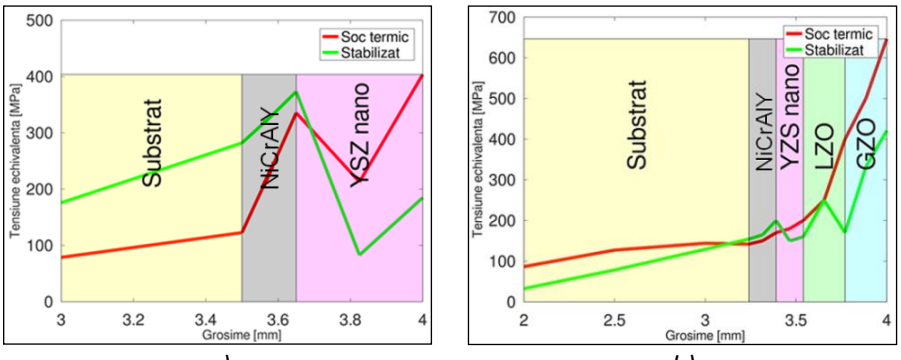

Fig. 6.4 *Distribution of von Mises stresses: (a) in the system (E2T3) and (b) in system E2T7*

Tab. 6.1 *Maximum values of von Mises equivalent stresses in E2T2-E2T7 systems*

Sisteme	E2T2	E2T3	E2T4	E2T5	E2T6	E2T7
Valorile max. tensiuni von Mises [MPa]	390	373	416	415	393	421

The thermo-structural simulation results indicated that systems with TBC coatings consisting of Zr oxides with La and Gd (E2T4-E2T7) had the highest temperature drops on the substrate (v. Fig. 6.3.c, but also the highest von Mises stresses (see Table 6.1). Although the lanthanum (LZO) and gadolinium (GZO) zirconate have the most effective thermal barriers, these systems are also the most susceptible during thermal cycling to exfoliation due to the stresses induced by the significant differences between the thermal expansion coefficients of the metallic bond coat (~15 x $10^{-6}C^{-1}$) and Zr oxide with rare earth layers (9-10 x $10^{-6}C^{-1}$). At the opposite in terms of stresses was the TBC system with nanostructured YSZ (E2T3) (see Tab. 6.1), which had a 31°C higher temperature drop across the substrate than the conventional YSZ coated system (E2T2) (see Fig. 6.3.c).

Due to the anisotropic nature of thermally sprayed coatings and the internal stresses induced by the formation (during oxidation) of the TGO layer at the metal/ceramic layer interface, simulation-based judgements on the behaviour of these systems during high-temperature exposure can only be made to a certain extent. Therefore, under similar or more severe conditions than operating conditions (isothermal oxidation and thermal shock), physical testing remains the most effective and reliable method for evaluating the performance of a TBC coating.

6.2 Manufacturing and preparation of support samples

The experimental models of substrate/TBC coatings were manufactured to validate the results from the numerical simulation. The experimental models of TBC coatings (see Fig. 6.1) were deposited by thermal plasma spraying under atmospheric conditions (APS) on laminated IN 625 alloy support samples that were water-jetted from a 1000 x 170 x 3 mm plate (Fig. 6.5.a-b) and on additively fabricated IN 625 alloy support samples (Fig. 6.5.c-d) with optimised process parameters (see § 5.2).

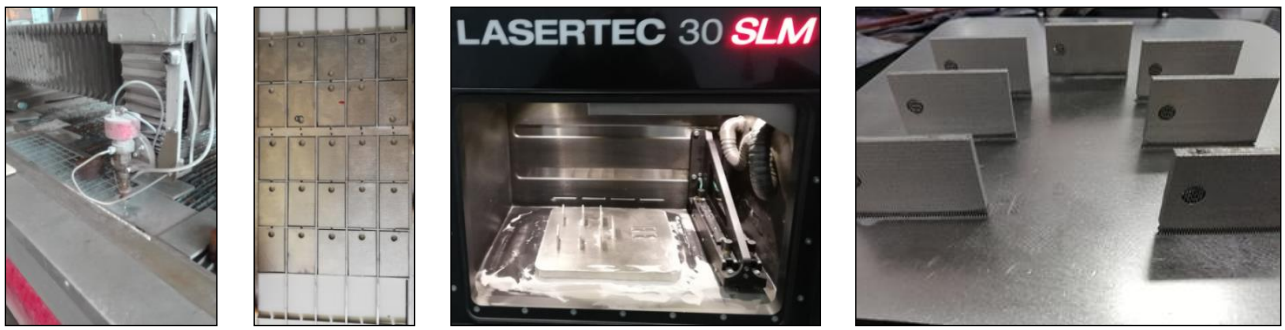

a) *b)* *c)* *d)*

Fig. 6.5 *Manufacturing of IN 625 support samples: (a-b) water jet cutting of laminated IN 625 alloy sheet samples and (c-d) additive manufacturing by SLM technology of IN 625 alloy samples*

6.3 Manufacturing of the experimental TBC coatings models

Before deposition of the TBC coatings, the support samples were cleaned, sandblasted and checked for surface quality and roughness. The morphology and chemical compositions of the

powders used for thermal deposition of coatings were analysed by microstructural (Fig. 6.6.a) and micro composition (Fig. 6.6.b) investigations using scanning electron microscopy and X-ray energy dispersive spectroscopy (SEM-EDS).

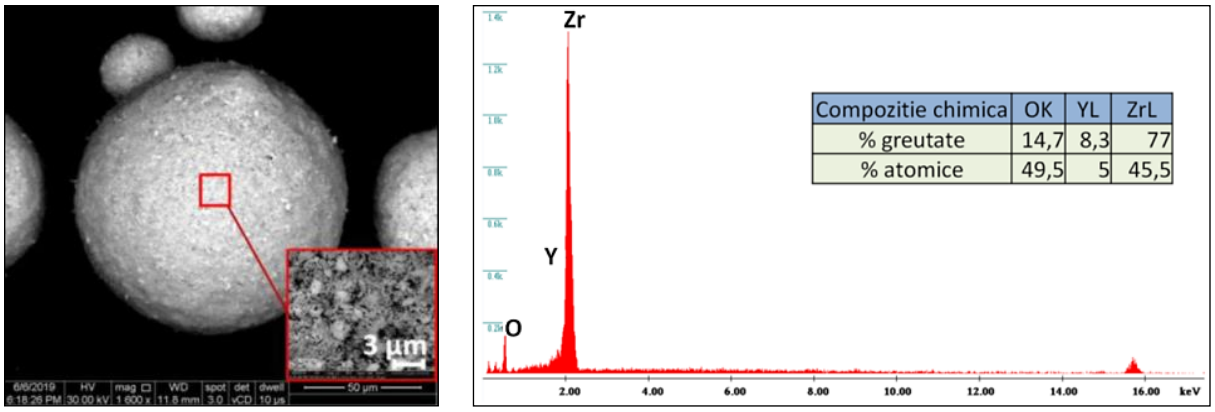

a) *b)*

Fig. 6.6 *Analysis of nanostructured YSZ ceramic powders: (a) SEM image (Paraschiv A. 2020c) and (b) chemical composition of particles based on EDS spectra*

A Metco 7M plasma spraying system was used to produce the TBC coatings. The spray gun was controlled by a KUKA industrial robot pre-programmed for each coating configuration (Fig. 6.7.a-c).

a) *b)* *c)*

Fig. 6.7 *Manufacturing of experimental models of TBC coatings: (a) thermal spraying equipment using APS technology; (b) thermal spraying of coatings; and (c) IN 625 samples with TBC coatings.*

The experimental models of TBC coatings (Fig. 6.8) were deposited by (APS) technology, changing certain process parameters such as electrical intensity and voltage, spray distance and process gas pressure. The experimental models of TBC coatings were deposited in three deposition campaigns resulting in 44 samples.

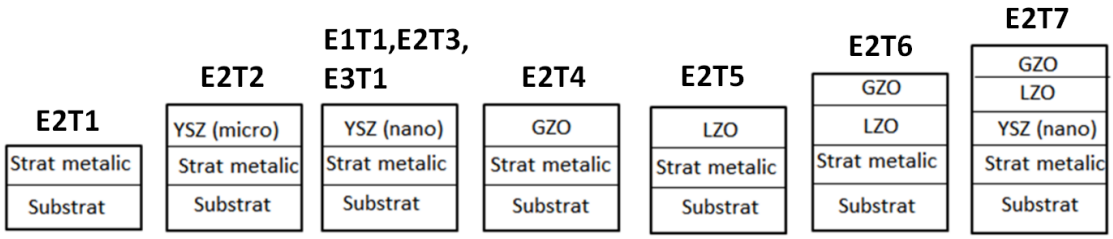

Fig. 6.8 *Experimental models of TB coating obtained by thermal spraying*

Chapter 7. Theoretical and experimental contributions to the high-temperature testing and characterisation of substrate/TBC coating systems

7.1 Oxidation testing of substrate/TBC coating systems

To achieve the objective of developing innovative TBC coatings and thermal spray technology to protect the additively manufactured turbine blade, experimental models of substrate/ TBC coating systems were tested under laboratory conditions close (cyclic oxidation) and much more severe (thermal shock) than those during service.

Cyclic oxidation test conditions consisted of heating the samples at a rate of 10°C/min to 1100°C and maintaining them for six 100-hour cycles. At each oxidation cycle, one sample was extracted from each type of coating and investigated. After the first oxidation cycle, the substrate/ TBC coating systems with lanthanum (LZO) and gadolinium (GZO) zirconate were prematurely exfoliated at the metallic bond coat/ceramic layer interface. On the other hand, systems with YSZ-layer coatings (conventional and nanostructured) maintained their structural integrity even after six oxidation cycles at 1100°C, with no delaminations, exfoliations or macrocracks identified. Analysing the fracture zone of the coatings and taking into account the findings from the simulation of the thermo-mechanical behaviour of systems with lanthanum La (LZO) and Ga (GZO) zirconate (see § 6.1), the leading cause of the exfoliation of these coatings was the high level of internal stresses at the interface between the metallic bond coat or the YSZ layer (depending on the type of system) and LZO and/or GZO layer(s). Other factors that favoured the exfoliation of thermally sprayed coatings were the layers' low adhesion/cohesion resistance (*Paraschiv A. et al. 2018c*), the high thickness and low porosity of the GZO and LZO layers. However, at the national level, no studies on thermal spray deposition of TBC coatings with LZO, GZO and nanostructured YSZ coatings have been identified, and the technological maturity level for deposition of these coatings is low and requires further research.

The research on the testing and characterisation of the oxidation behaviour of the developed experimental designs continued on samples of ceramic coated TBC coatings of conventional YSZ and nanostructured YSZ, using as reference systems samples of laminated and additively fabricated IN 625 with and without metallic coating. The substrate/TBC coating systems, in their as-built state and after each oxidation cycle, were analysed in detail in terms of mechanical behaviour and bond coat roughness evolution. Also, the evolution of the increased oxide layer thickness (TGO) and the porosity of the ceramic layer was analysed, and the experimental data were subsequently used to perform a comprehensive analysis of the oxidation kinetics at high-temperature of experimental models of TBC substrate/coating systems.

7.2 Mechanical behaviour of additively laminated and fabricated alloys

Microstructural investigations investigated the effects of long-term oxidation at 1100°C on the mechanical behaviour of the two IN 625 alloys (laminated and additively fabricated), and Vickers microhardness tests (HV 0.3) carried out with Vickers Wolpert Wilson® Instruments 402 MVD equipment according to ASTM E384-10e2 (**** ASTM E384-10e2 2010*).

The SEM investigations revealed that the oxide surface layer forming on the alloy surface became brittle after three oxidation cycles (300 hours) in the absence of a protective coating, allowing oxygen to diffuse into the substrate to a depth of more than 100 µm after six oxidation cycles in both the laminated (Fig. 7.1.b) and additively fabricated (Fig. 7.2.b) alloys.

Similarities were also observed in the mechanical behaviour of these two alloys. The laminated and additively fabricated alloy had appropriate average Vickers microhardness values in the initial state, i.e. 260±22 HV0.3 and 258±18 HV0.3. However, as the oxidation time increased, an ageing effect occurred on both alloys, causing an increase in microhardness of about 10% compared to the initial state (Fig. 7.1.c, Fig. 7.2.c).

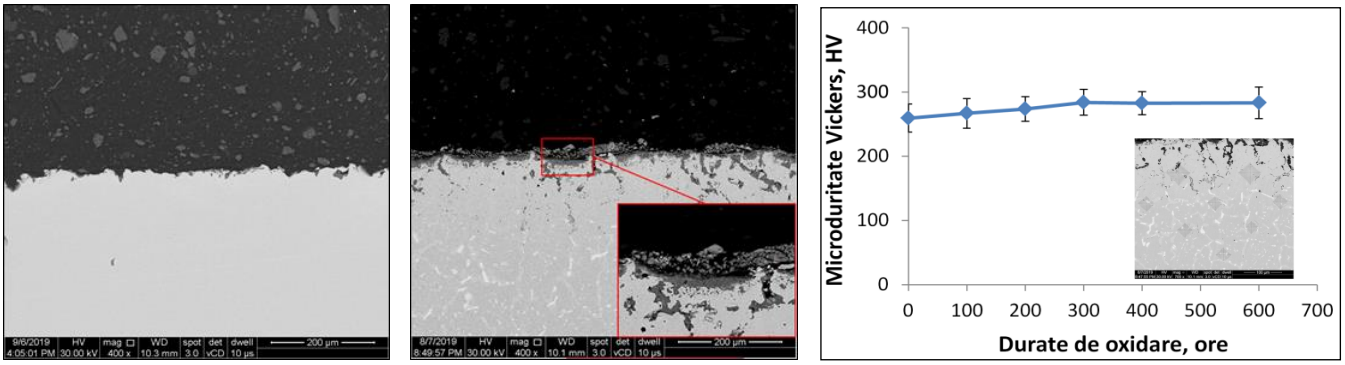

a) *b* *c)*

Fig. 7.1 *Effects of high-temperature oxidation on laminated IN 625 alloy: (a-b) SEM images of the microstructure in the initial state and after 600 hours of oxidation and (c) Vickers microhardness evolution*

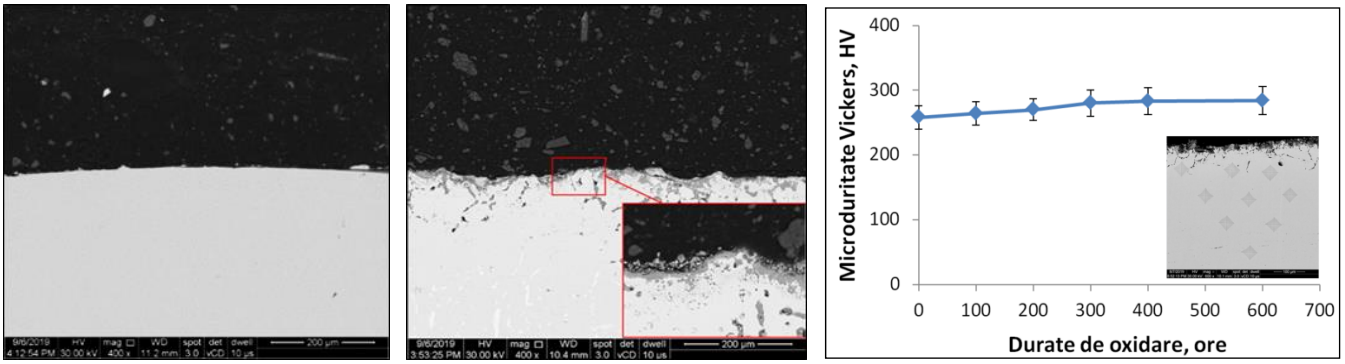

a) *b)* *c)*

Fig. 7.2 *Effects of high-temperature oxidation on additively fabricated IN 625 alloy: (a-b) SEM images of microstructure in the initial state and after 600 hours of oxidation and (c) Vickers microhardness evolution*

7.3 Mechanical behaviour of the metallic bond coat

Microstructural analyses carried out in the cross-section of samples with the metallic bond coat (without ceramic layer) revealed that exposure to high temperatures for extended periods promoted an accentuation of the oxidation process, leading to a significant decrease in thickness of the bond coat after 600 hours of oxidation (Fig. 7.3.b).

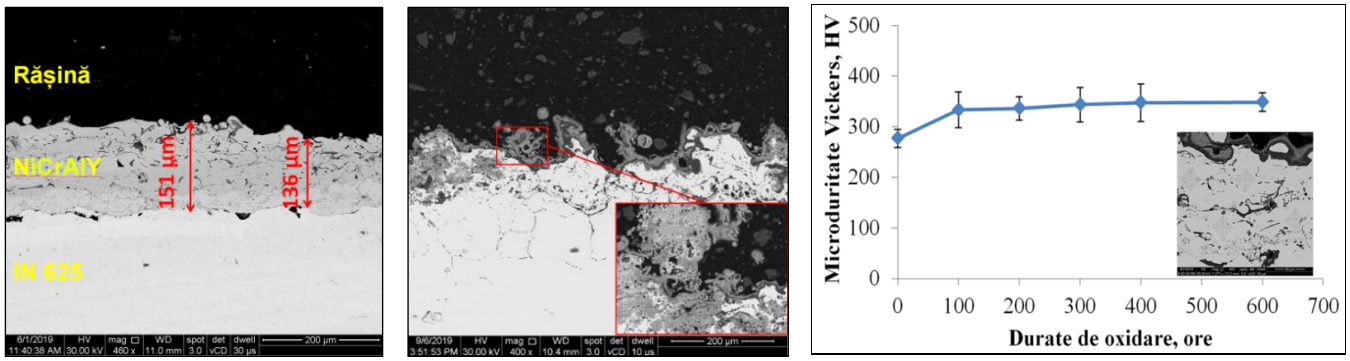

a) *b)* *c)*

Fig. 7.3 *Effects of high-temperature oxidation on the NiCrAlY alloy bond coat: (a-b) SEM images of the microstructure in the initial state, (b) after 600 hours of oxidation and (c) Vickers microhardness evolution*

As in the case of the substrate, the age-hardening effect resulting from oxidation was also observed in the case of the NiCrAlY bond coat, when the microhardness increased after oxidation by more than 25% compared to the initial state (277 HV0.3). Oxygen in the atmosphere reacts with the aluminium present in high concentrations in the *β*-phase precipitates of the metal layer, forming a thin layer of alumina (Al_2O_3) on its surface, known in the literature as thermally grown oxide layer (TGO) (*A. Banu, A. Paraschiv et al. 2020*). The TGO layer copies the surface profile of the metal layer and accentuates its protrusions (increases its roughness) as it increases in thickness, inducing internal stresses at the bond coat/TGO/ceramic interface.

7.4 Surface roughness evolution at the substrate/TBC coating interface

Conventional methods used to measure surface roughness (mechanical palpation, interferometry and stereomicroscopy) (*Paraschiv A. et al. 2016*) do not apply to surfaces that are already coated, such as the metallic bond coat in substrate/TBC coatings systems.

This drawback contributed to the motivation to develop in this PhD thesis a methodology for non-contact assessment of metallic bond coat roughness based on imaging techniques, graphical representations and numerical computation. This methodology involves the use of equipment/tools to perform the following operations:

(I) cutting and metallographic preparation of the TBC coated sample;
(II) capture and processing of scanning electron microscopy (SEM) images in *.tif* format;
(III) determination of the roughness profile from the processed SEM images;
(IV) calculating roughness parameters;
(V) verification of the measurement accuracy of the method.

Initially, the TBC-coated sample is cross-sectioned, hot encapsulated in an epoxy resin, metallographically prepared and introduced into the scanning electron microscope. For surface roughness analysis over the whole cross-section of the sample, 12 SEM images (at x300 magnification) were captured in different fields at the metal/ceramic layer interface and then binarised in Matlab. After the binarisation of the SEM images (Fig. 7.4.a-c), the spatial coordinates of the roughness profile of the bond coat, initially expressed in pixels and transformed into micrometres, are determined by iterative programming performed in Matlab (Fig. 7.4.d), based on which the profile of the surface of interest is obtained as a vector.

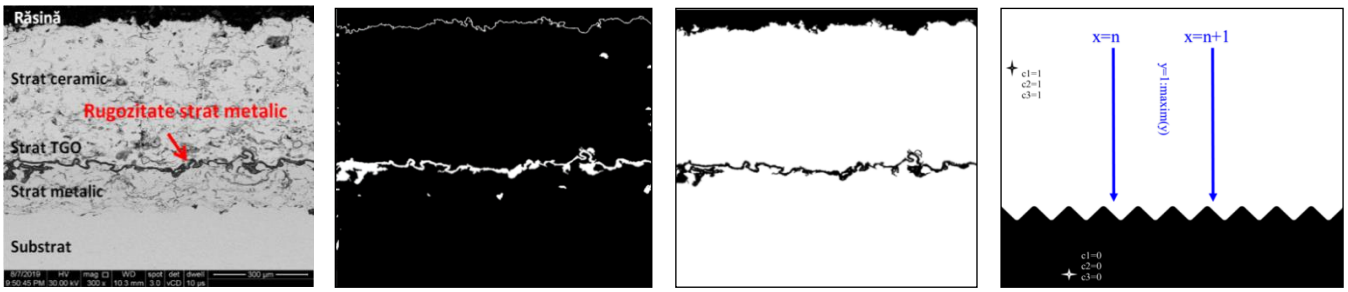

a) *b)* *c)* *d)*

Fig. 7.4 *SEM image binarization with a cross-section of a sample with TBC coatings: (a) raw image and (b) binarised image after one iteration (Paraschiv A. et al. 2021)*

To obtain the median line of the roughness profile (vector), according to which all roughness parameters are calculated, four alternative filters to the conventional filters (2CR, ISO 2CPC and Gaussian) were analysed in the proposed methodology (*Whitehouse D. 2002*): three filters taken from the Matlab database (digital filter - Relation 7.1, normalisation filter - Relation 7.2 and moving averaging filter - Relation 7.3) and one filter proposed by *Helminiak M.A. et al.* (*2008*) (averaging filter - Relation 7.4) (see also the sequence in Code 1 - Matlab, Fig. 7.5.b). After determining the median line of the roughness profile, the dimensional deviations from a reference line are calculated using Relation 7.5.

$$m(t) = \frac{1}{windowSize}\Big(y(t) + y(t-1) + \cdots + y\big(t-(windowSize-1)\big)\Big) \quad (7.1)$$

$$medie\_vector = \frac{y(1)+y(2)+y(3)+\cdots y(n)}{n} \quad (7.2)$$

$$m = \frac{y(1)+y(2)+y(3)+\ldots+y(n)}{n} \quad (7.3)$$

$$k(i) = \frac{y(i-1)+y(i)+y(i+1)}{3} \quad (7.4)$$

$$r = y - m \quad (7.5)$$

Where: *m* is the middle line, *y* is the spatial vector of the vertical profile, *t* is the iteration, *n* is the length of the vector, *i* is the interval of the profile, *k* is the parameter that determines the values that an interval will have, and *r* is the vector containing the dimensional deviations.

After calculating the dimensional deviations (Relation 7.5), the roughness parameters Ra, Rp, Rq and Rz are calculated. For a correct comparison of the results obtained using the developed methodology with the results obtained using a conventional roughness measuring instrument (MarSurf PS 10), the roughness parameter formulae according to BS EN ISO 4287:2000 were applied. In addition, the roughness parameter formulas were adapted for the Matlab code, an example being the Ra parameter, whose specific formula was adapted in Matlab (Relation 7.6).

$$Ra = \frac{1}{l}\int_0^l |Z(x)|dx \quad \xrightarrow{\textit{adapted in the program}} \quad Ra = \frac{r(1)+r(2)+r(3)+\ldots+r(n)}{n} \quad (7.6)$$

The roughness profile generated by a conventional instrument on the surface of a roughness standard with nominal value Rz=9.686 µm was processed in Matlab to validate the methodology and

verify the measurement accuracy. By applying the digital filter (Relation 7.1), a deviation of the calculated Rz parameter from the nominal Rz of 0.64% (Rz=9.748 µm) was obtained (Fig. 7.5.a).

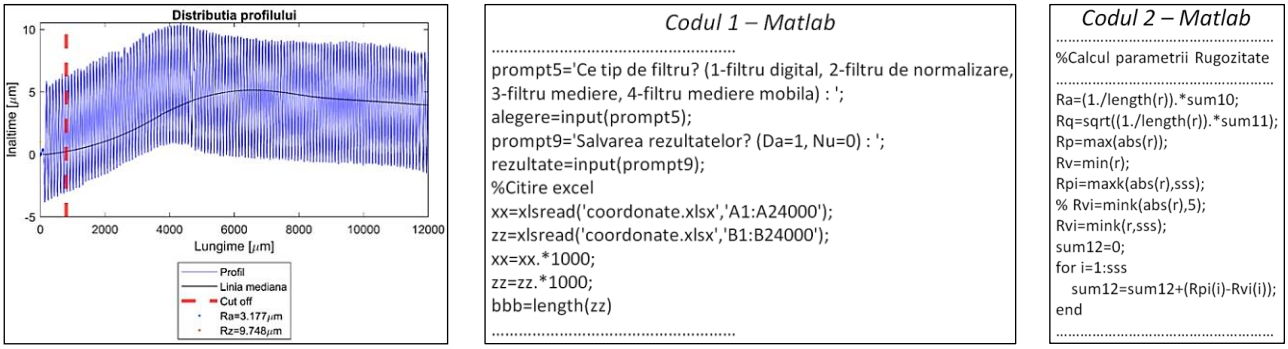

a) *b)* *c)*

Fig. 7.5 *Applying the non-contact roughness assessment methodology: (a) determination of the roughness profile median line (adapted from Paraschiv A. et al. 2021); (b-c) Matlab code sequences 1 and 2*

The developed methodology was applied to analyse the evolution of the roughness parameters Ra, Rz, Rp and Rq of the bond coat in substrate/coating TBC systems with conventional YSZ and nanostructured YSZ ceramic layer in the initial state and after each 100-hour oxidation cycle at 1100°C (see also the sequence in Code 2 - Matlab, Fig. 7.5.c). In addition, 12 SEM images were captured at x300 magnification for each sample to analyse the entire coating interface.

Fig. 7.5.a compares the average values (obtained from 12 values) of the Ra roughness of the bond coats in the systems with conventional YSZ and nanostructured YSZ in the initial state and after each oxidation cycle. SEM images and schematic representations of the evolution of the bond coat prominences after one cycle and after six oxidation cycles at 1100°C are shown in Fig. 7.6.b.

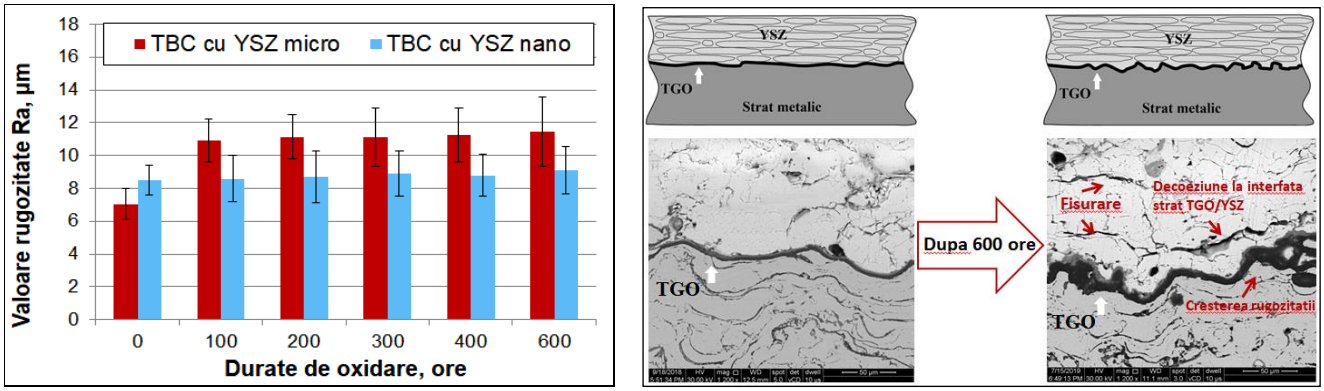

a) *b)*

Fig. 7.6 *Evolution of bond coat surface roughness in the conventional YSZ and nanostructured YSZ systems after oxidation testing at 1100°C: (a) evolution of Ra roughness and (b) illustration of the effects induced by increasing roughness at the bond coat/ceramic layer interface (adapted from Paraschiv A. et al. 2021)*

The roughness parameter values generally followed the same increasing trend with increasing oxidation times due to increasing TGO layer and mixed oxides, higher in the conventional YSZ system than in the nanostructured YSZ system.

Developing a methodology for non-contact measurement of the roughness parameters (Ra, Rz, Rq and Rp) of the metallic bond coat helps to understand better the effects of oxidation on the components in a substrate/TBC coating system. Also, it can provide information on the optimal surface roughness that the surface of the metallic bond coat should have in an initial state and a prediction of the system's behaviour during oxidation.

7.5 Oxidation behaviour of the ceramic top coats

7.5.1 Vickers microhardness

High-temperature oxidation of TBC coating systems produces a densification effect that reduces porosity, improves layer cohesion and increases the hardness of ceramic layers. The initial-state microhardness value of conventional YSZ and nanostructured YSZ layers was 594±99.3 HV0.3 and 734±96 HV0.3, respectively, and after six oxidation cycles, it increased by about 25% and 45%, respectively (Fig. 7.7.a-b).

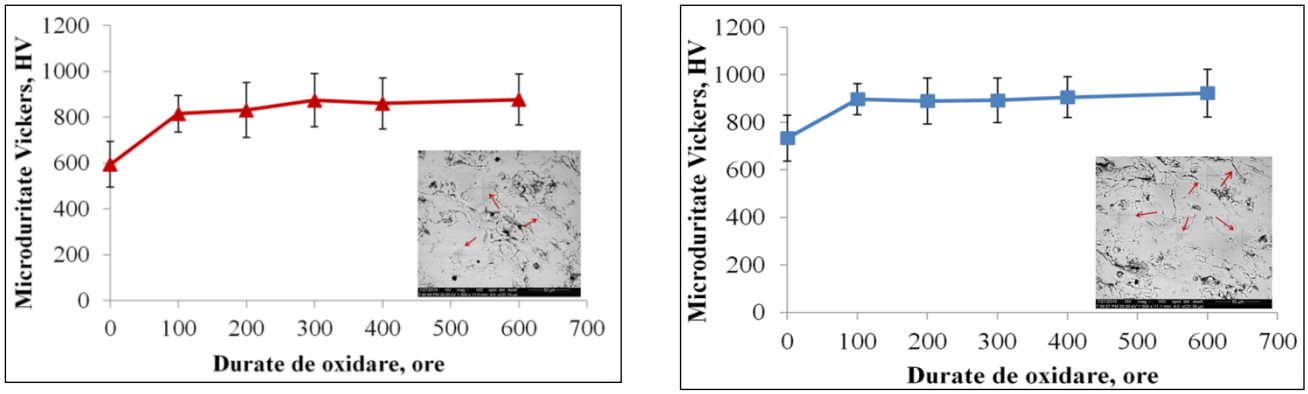

a) *b)*

Fig. 7.7 *Effect of oxidation at 1100°C on ceramic layer microhardness: (a) from conventional YSZ and (b) nanostructured YSZ*

A particularity of ceramic coatings also observed through the high degree of scattering in the microhardness test values (see Fig. 7.7.a-b) is the susceptibility of these brittle materials to crack easily after indentation.

7.5.2 Fracture toughness

By correlating the average length of the diagonals of the Vickers indentation with the average length of the cracks that form when a critical load is exceeded near or at the peaks of the indentation, another critical mechanical property of thermal spray deposited mechanical coatings, called fracture toughness (*KIC*), can be assessed (*Paraschiv A. et al. 2015, 2018c*).

The layers of conventional YSZ and nanostructured YSZ (in the initial state) were preliminarily tested with four indentation loads (50, 100, 200 and 300 gf) to evaluate crack propagation as a function of indentation load. The crack lengths were measured using scanning electron microscopy (SEM) and the dedicated SEM image processing software Scandium 5.2. Preliminary experimental results showed a linear increase in average crack length with increasing indentation loads. In both

types of layers, the cracks were of the Palmqvist type (*Evans A.G. and Charles E.A. 1976*), and the formula used to determine the fracture toughness is described by Relation 7.7.

$$K_{IC} = 0.16HV \cdot a^{\frac{1}{2}} \cdot \left(\frac{c}{a}\right)^{-\frac{3}{2}} \qquad (7.7)$$

Where: *KIC* is the fracture toughness (MPa·m$^{1/2}$), *HV* is the Vickers microhardness value (Gpa), *c* is the sum of the average crack length and the average diagonal of the indentation (mm), and *a* is half of the average diagonal of the indentation (mm).

Using Relation 7.7, the average values (obtained from 20 values each) of the fracture toughness of conventional YSZ and nanostructured YSZ layers in the initial state and after each oxidation cycle are shown in Fig. 7.8.a.

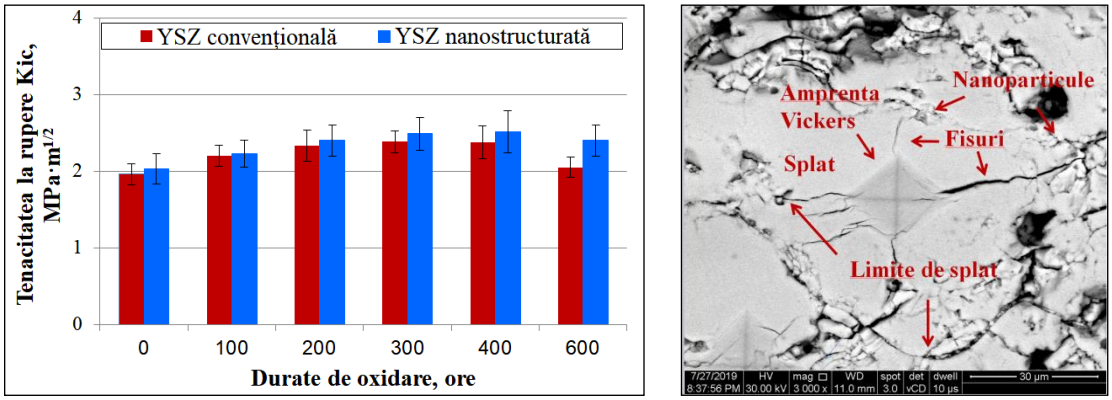

a) *b)*

Fig. 7.8 *Comparative analysis of fracture toughness of conventional YSZ and nanostructured YSZ ceramic layers as a function of increasing oxidation times and (b) Vickers microhardness impression and typical cracks resulting from the indentation of nanostructured YSZ ceramic layer*

Throughout the oxidation tests, the fracture toughness of the nanostructured YSZ layer was higher than that of the conventional YSZ layer due to the agglomerations of nanoparticles in the YSZ nanostructured that prevented crack propagation (see Fig. 7.8.b) and delayed the sintering effect of the YSZ by at least 100 hours.

7.5.3 Porosity

The porosity evolution of conventional YSZ and nanostructured YSZ ceramic layers in oxidation tested systems was analysed using a methodology developed in the thesis for the quantitative measurement of pores in ceramic layers based on SEM image processing. By binarising SEM images taken in the cross-section of TBC coatings (Fig. 7.9.a), pores and even nanopores (which cannot be detected by conventional methods) in the coating can be quantitatively measured based on the quantification of their associated pixels and the ratio of their area to the whole analysed area (*Paraschiv A. et al. 2018a*).

The developed methodology was used to analyse the porosity evolution after different oxidation cycles of conventional YSZ (E2T2 system) and nanostructured YSZ (E1T1 system), which had an initial porosity of 16.17% and 12.87%, respectively. Additionally, two nanostructured YSZ layered

systems, E2T3 and E3T1, were analyzed, having an initial state porosity of 20.92% and 16.21%, respectively (Fig 7.9.b).

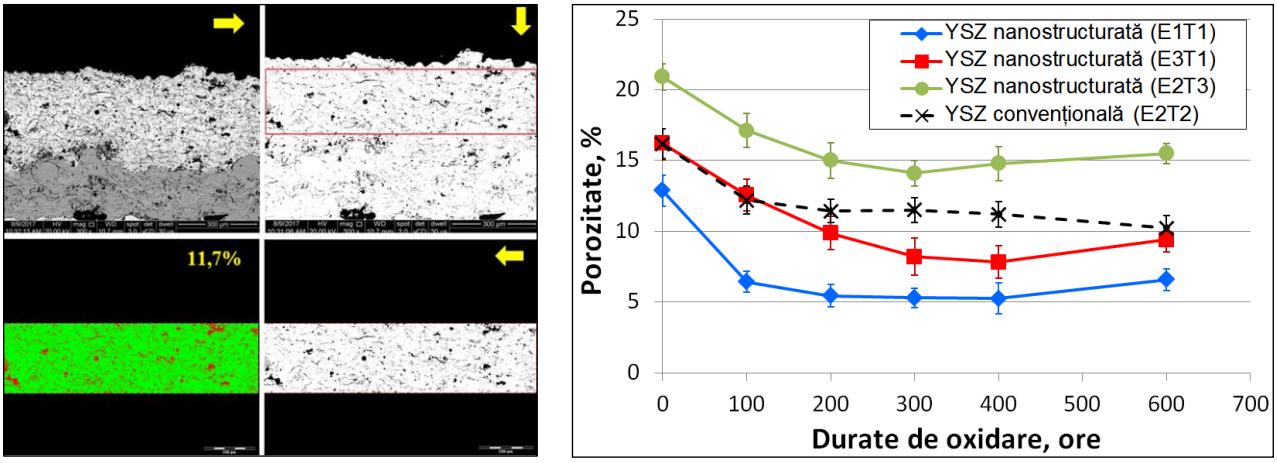

a) *b)*

Fig. 7.9 *Porosity assessment of ceramic layers after oxidation at 1100°C: (a) SEM image processing for quantitative porosity determination and (b) porosity evolution in ceramic layers of conventional YSZ (E2T2) and nanostructured YSZ (E1T1, E2T3, E3T1) (adapted from Paraschiv A. et al. 2020c)*

In all cases, after the first oxidation cycle (100 hours), the porosity of the ceramic layers was reduced by more than 20% compared to the initial state. A low level of porosity in the ceramic layer of a TBC coating has a negative impact on the efficiency and lifetime of TBC coatings because it decreases the deformation tolerance and increases the thermal conductivity of the coating. Therefore, it is preferable to maintain as high porosity as possible during thermal cycling. In this case, the advantage of nanostructured YSZ coated TBC coatings (E1T1, E2T3 and E3T1) is given by the bimodal structure (nano- and micrometric structure) whose nanoparticle agglomerations have a higher shrinkage than adjacent areas with lamellar structures (micrometric structure), forcing the growth of pore and discontinuities between the two types of structures. (*Baiamonte L. et al. 2015*).

7.6 Oxidation behaviour of thermally grown oxide layer (TGO)

The research continued with analysing the thermally grown oxide layer (TGO) in the conventional YSZ and nanostructured YSZ systems.

In Figs. 7.10-7.11, cross-sectional SEM images of the conventional YSZ system (E2T2) and the nanostructured YSZ system (E1T1) are shown in the initial state and after 100, 200, 300, 400 and 600 hours of holding at 1100°C.

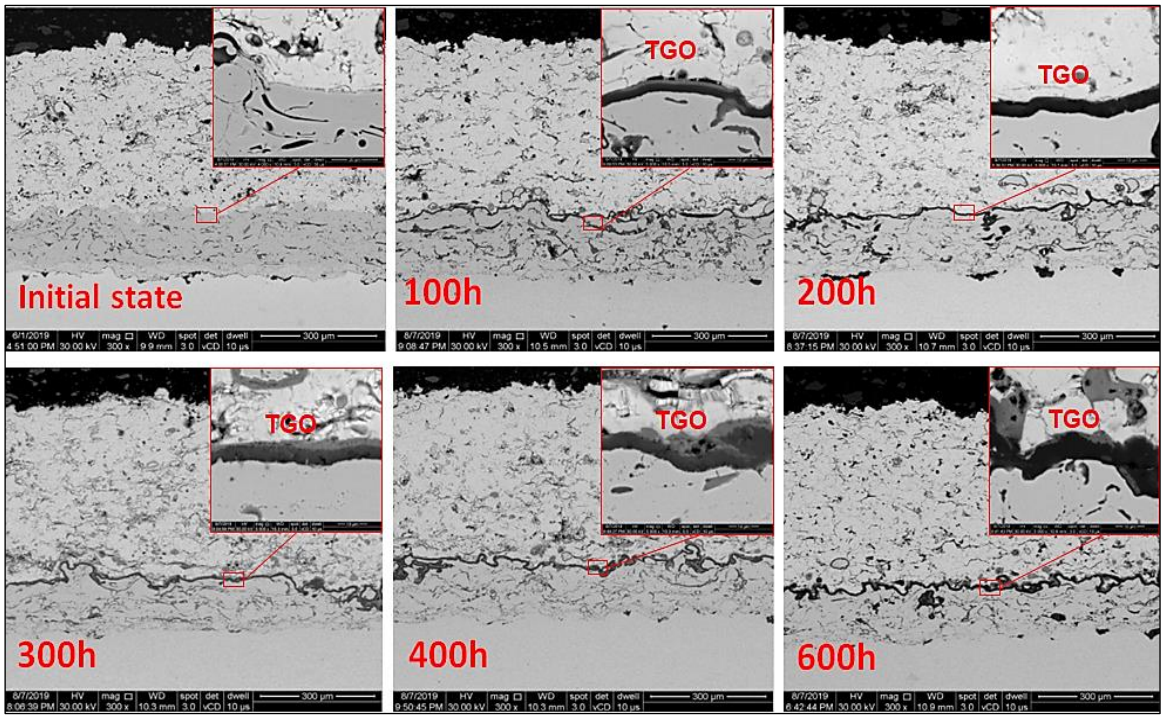

Fig. 7.10 *Cross-sectional SEM images of TGO layer evolution in conventional YSZ (E2T2) systems after exposure at 1100°C oxidation cycles (Paraschiv A. et al. 2020c)*

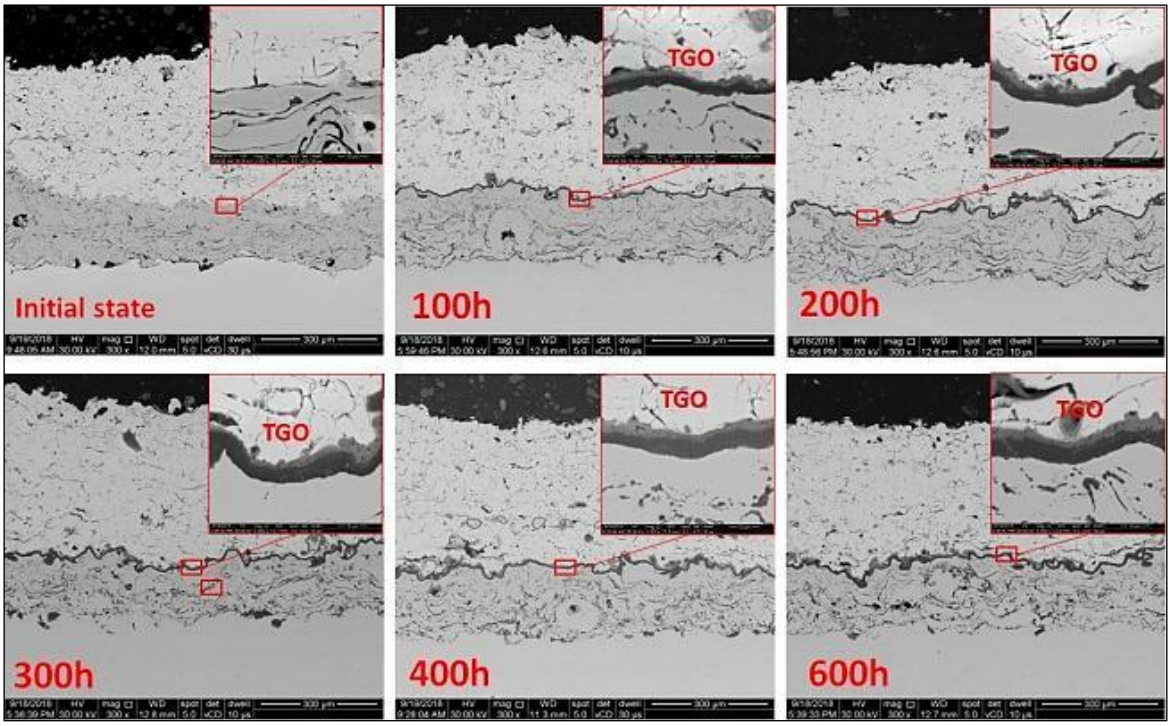

Fig. 7.11 *Cross-sectional SEM images of TGO layer evolution in nanostructured YSZ (E1T1) systems after exposure at 1100°C oxidation cycles* (*Paraschiv A. et al. 2020c*)

For each type of coating, 12 SEM images were taken after each oxidation cycle to assess the average thickness of the TGO layer over the entire cross-section of a coating. In each SEM image, the

TGO layer was measured at 5 points at approximately 50 µm intervals. Fig. 7.12 shows the average values of TGO layer thickness as a function of oxidation time, where each point represents the average of 60 measurements.

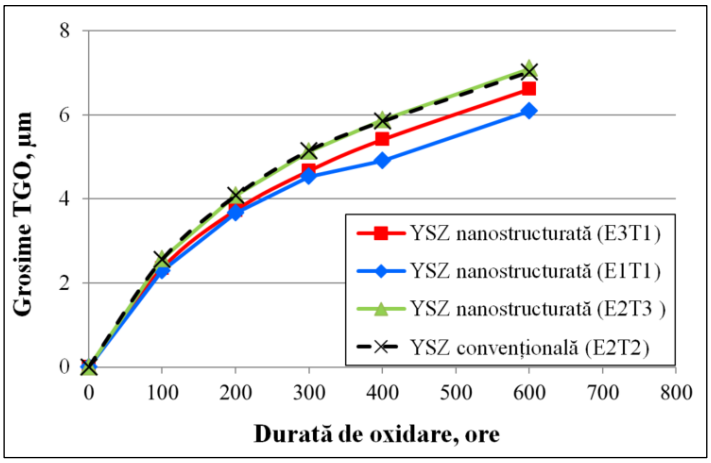

Fig. 7.12 *TGO oxide layer thickness evolution in conventional YSZ (E2T2) and nanostructured YSZ (E1T1, E2T3, E3T1) ceramic layer systems after oxidation at 1100°C*

The TGO oxide layer showed in all cases the same trend of increasing thickness with increasing oxidation times (Fig. 7.12), following a parabolic law, which is typical for the TBC coatings exposed for long durations at temperatures above 1000°C (*Keyvani A. et al. 2012*, Lima R.S. and Marple B.R. 2008, *Sun J. et al. 2010*). From the analysis of the experimental data, it was observed that a Gaussian distribution could model the TGO layer thickness values. Figs. 7.13 are graphically represented the normal probability distributions of the TGO layer thicknesses in the systems with conventional YSZ layer (E2T2) and nanostructured YSZ layer (E1T1, E2T3, E3T1) after six oxidation cycles at 1100°C. In Fig. 7.14.a-b, the TGO layer thicknesses of the conventional YSZ (E2T2) and nanostructured YSZ (E1T1) layered system are shown individually after each oxidation cycle at 1100°C.

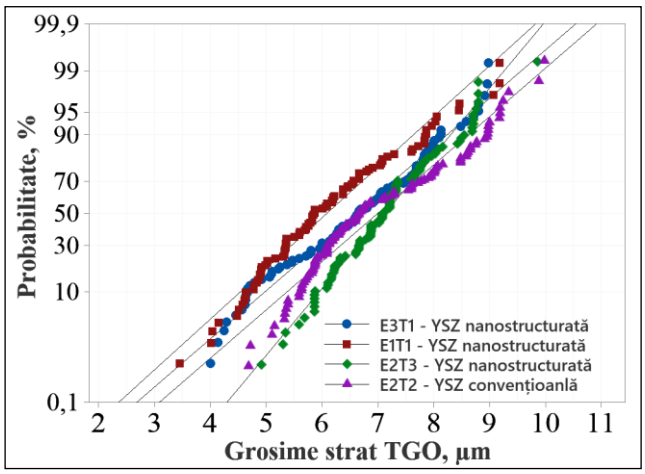

Fig. 7.13 *Probability distribution plots of TGO layer thickness in conventional YSZ (E2T2) and nanostructured YSZ (E1T1, E2T3, E3T1) systems after six oxidation cycles at 1100°C*

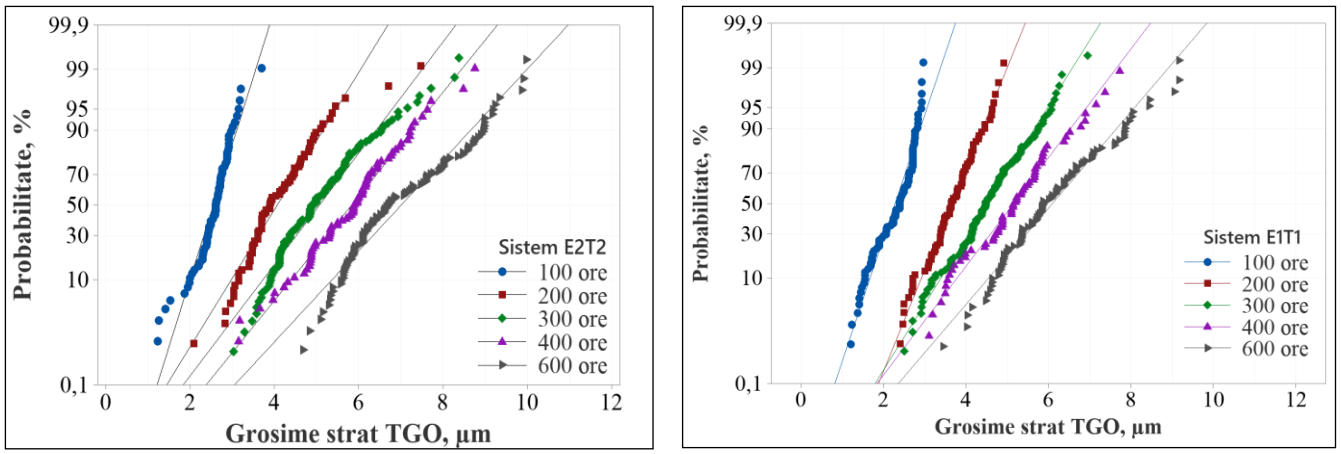

a) *b)*

Fig. 7.14 *Probability distribution plots of TGO layer thickness after each oxidation cycle at 1100°C in systems: (a) with conventional YSZ layer (E2T2) and (b) with nanostructured YSZ layer (E1T1)*

Although the two types of layers show considerable differences in TGO layer thickness, analysis of the histograms in Fig 7.14.a-b reveals that the probability distributions of TGO layer values showed similar trends with increasing oxidation duration. Also, in both cases, an increase of the standard deviations was observed, which indicates a non-uniform growth of the oxide layer (especially after 600 hours), the possible causes being: (i) different orientation of the alumina grains; (ii) the more pronounced formation of the mixed oxides in areas with defects, cracks, pores etc.; (iii) non-homogeneous growth of the layer. These possible causes are also supported by microstructural and micro composition analyses (SEM-EDS) of the TGO layer in the system with conventional YSZ and nanostructured YSZ. The SEM images and chemical element distribution maps of the system with conventional YSZ (E2T2) after six oxidation cycles are shown in Fig. 7.15.a-b.

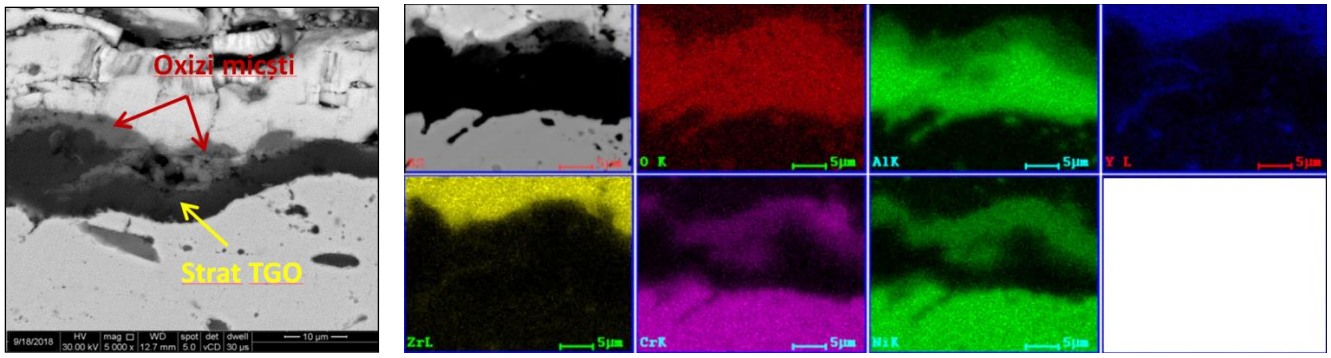

a) *b)*

Fig. 7.15 *SEM cross-sectional image and chemical element distribution maps at the metal layer/TGO layer/ceramic layer interface of the system (E2T2) with conventional YSZ layer after six oxidation cycles (Paraschiv A. et al. 2020c)*

The EDS analysis revealed that the TGO layer consisting mainly of oxygen and aluminium (Al_2O_3) is covered after six cycles by a thin and irregular layer of mixed oxides (spinels) such as $NiCr_2O_4$ and $NiAl_2O_4$, resulting from the diffusion and reaction of Cr and Ni with oxygen and other compounds (Cr_2O_3, Al_2O_3 and NiO) (*Liu X. et al. 2016*, *Girolamo G. D. 2016*, *A. Banu*, *A. Paraschiv et al. 2020*).

7.7 Theoretical contributions to the kinetics of the high-temperature oxidation process of experimental models of TBC substrate/coating systems

7.7.1 Oxidation kinetics

Oxidation kinetics at 1100°C of conventional YSZ (E2T2) and nanostructured YSZ (E1T1, E2T3, E3T1) ceramic layer systems were analysed based on the TGO layer evolutions (see Fig. 7.12). Since, in all cases, the increase in thickness of the TGO layer followed a parabolic function, the oxidation kinetics can be described by Relation 7.8 (*Pimin Z. 2018*).

$$d_{TGO} = kp\,(t_{Tmax})^{n} \qquad (7.8)$$

Where: *dTGO* is the average TGO layer thickness in meters, *t* is the time in hours, *kn* is the velocity coefficient expressed in µm/h$^{0.5}$, and *n* is the oxidation exponent.

Identifying a more accurate value of the oxidation exponent *n* is essential for an exact determination of the oxidation rate of the coating, but in most studies from the literature, a value of 2 is chosen to simplify the calculations. Therefore, a regression analysis was performed to determine the oxidation exponent value *n* for systems with conventional YSZ (E2T2) and nanostructured YSZ (E1T1, E2T3, E3T1). Several iterations were performed for *n* ranging from 1 to 3 until the value of the determination coefficient R^2 was closest to 1 to test the linearity of the model and the degree of the approximation polynomial. Fig. 7.16 shows the iterations based on which the oxidation exponents of the E1T1, E2T2, E2T3 and E3T1 systems were determined.

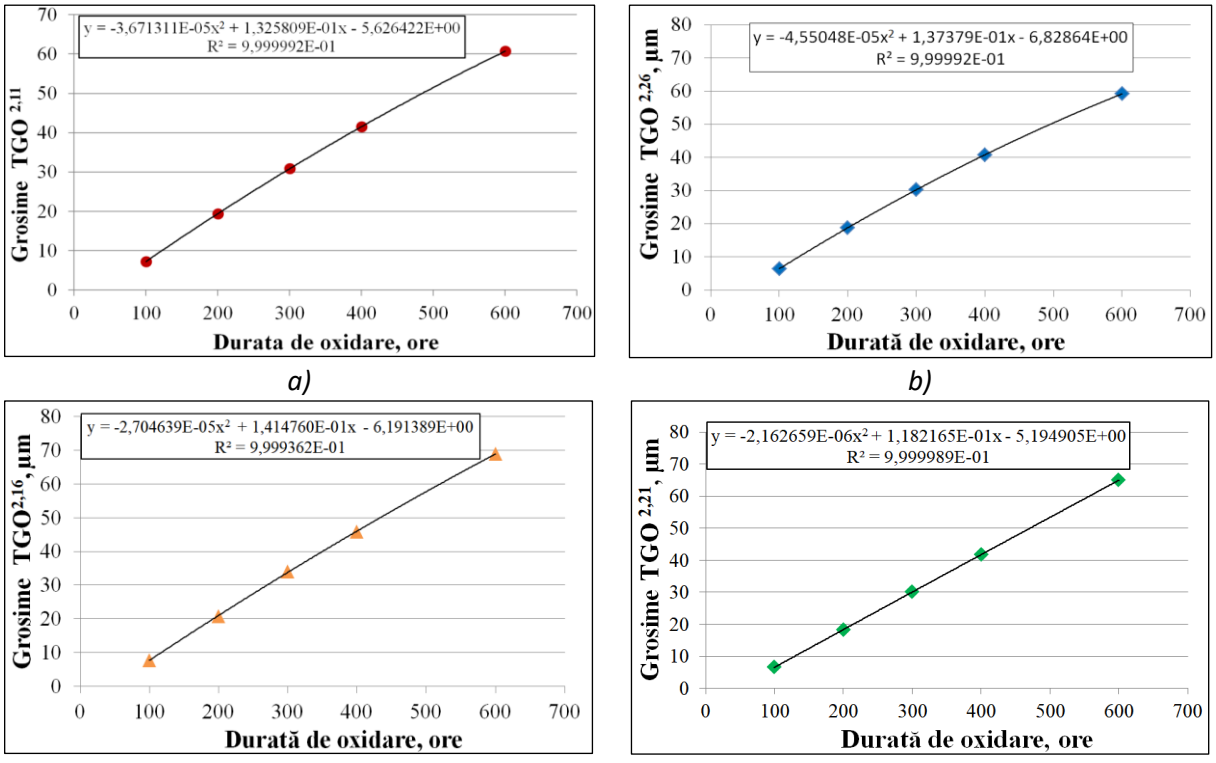

Fig. 7.16 *Determination of oxidation exponents: (a) system with conventional YSZ (E2T2, n=2.11) and (b-d) systems with nanostructured YSZ (E1T1, n=2.26; E2T3, n=2.16; E3T1=2.21)*

In all four systems, a value of the oxidation exponent *n* greater than 2 was identified (see Fig. 7.16.a-d), indicating that the oxidation kinetics follow a "sub-parabolic" law (*Jackson R. D. et al. 2011*). Based on the calculated values of the oxidation exponent *n* and applying the formula for calculating the oxidation rate (see Relation 7.8), the oxidation rates were calculated after each oxidation cycle at 1100°C, plotted as a function of oxidation time (Fig. 7.17.a) and plotted in 3D as a function of oxidation exponent n (Fig. 7.17.b).

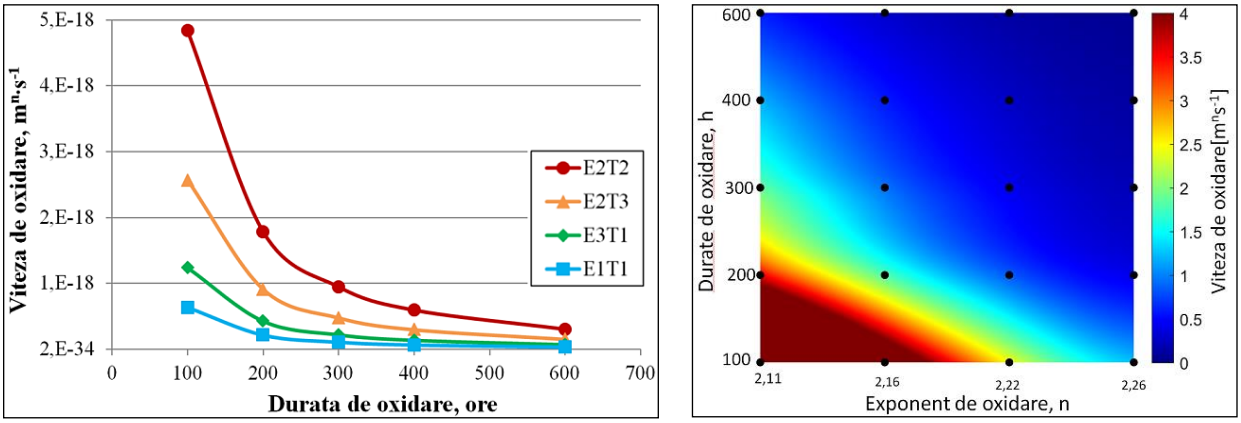

a) *b)*

Fig. 7.17 *Oxidation rates of systems with conventional YSZ (E2T2) and nanostructured layer YSZ (E1T1, E2T3, E3T1): (a) plot of oxidation rates versus time and (b) 3D plot of oxidation rate evolution versus time and oxidation exponent value n*

The growth rate of the oxide layer as a function of time in the four systems analysed could most correctly be expressed by a polynomial function of degree two. By determining the slope of the line for each curve (system) in Fig. 7.17.a, the oxidation rate constants were calculated, and their values are shown in Tab. 7.1. To compare the results with other results from the literature obtained on the same types of systems under similar conditions, the oxidation rate constants were also recalculated for the "standard" value 2 of the oxidation exponent n (see Tab. 7.1).

Tab. 7.1 *Oxidation rate constants of conventional YSZ and nanostructured YSZ systems*

References	YSZ type	Oxidation exponent, n - calculated	Oxidation rate, kn (n calculated), $m^n s^{-1}$	Oxidation exponent, n=2 (standard)	Oxidation rate constant, kn (n=2), $m^2 s^{-1}$	Oxidation rate constant, kn (n=2), $\mu m/h^{0.5}$
E2T2	conv.	2,11	5,9826E-18	2	2,42E-17	0,324
E3T1	nano.	2,21	1,5246E-18	2	2,19E-17	0,281
E1T1	nano.	2,26	8,0573E-19	2	2,18E-17	0,280
E2T3	nano.	2,16	3,1717E-18	2	2,42E-17	0,295
(*Jackson R. D. et al.2011*)	conv.	2,99	4,93E-23	2	1,92E-17	0,263
(*Keyvani A. et al. 2012*)	conv.	2,36	$0{,}5107 \cdot \sigma^{0{,}4218}$	-	-	-
	nano.	2,37	$0{,}4217 \cdot \sigma^{0{,}4190}$	-	-	-
(*Liu X. et al. 2016*)	conv.	-	-	2	3,29E-17	0,344
(*Keyvani A. 2015*)	nano.	-	-	2	1,22E-17	0,209
	conv.	-	-	2	2,78E-17	0,245
(*Daroonparvar M. et al. 2018*)	nano.	-	-	2	2,01E-17	0,269
(*Sezavar A. et al. 2019*)	nano.	-	-	2	2,62E-17	0,307
	conv.	-	-	2	3,01E-17	0,329

Analysis of the kinetics of the oxidation process revealed that the oxidation process in systems with nanostructured YSZ is slower than in systems with conventional YSZ due to the nanoparticle agglomerations and the bimodal layer structure of nanostructured YSZ that prevent oxygen diffusion to the metal layer and thus slow down the growth of the TGO layer (*Paraschiv A. et al. 2020c*, *Lima R.S. and Marple B.R. 2008*). Another factor with a strong impact on the oxidation behaviour of substrate/TBC coatings is the porosity of the ceramic layer, which at low values reduces the permeability of oxygen from the air, and at high values allows easier penetration of oxygen from the air to the metal layer (*Odhiambo J.G. et al. 2019*, *Rohnke M. et al. 2004*).

7.7.2 Influence of ceramic layer porosity on oxidation kinetics

The analysis of the experimental results obtained in the present PhD thesis indicated that between the initial porosity of the nanostructured YSZ ceramic layer, the oxidation exponent *n* and the oxidation duration, there is a close relationship represented 3D in Fig. 7.18.

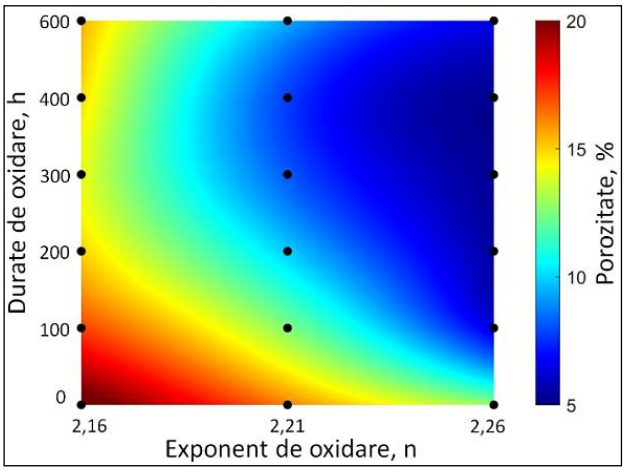

Fig. 7.18 *3D representation of the relationship between oxidation exponent and porosity of nanostructured YSZ ceramic layer as a function of increasing oxidation times at 1100°C*

The hypothesis that pores and cracks in the ceramic layer influence the oxidation behaviour of a TBC coating is unanimously accepted, but no studies have been identified in the literature presenting mathematical modelling of the influence of ceramic layer porosity on the oxidation kinetics of nanostructured YSZ in substrate/ TBC coating systems. The experimental results obtained in the PhD thesis and literature studies on the initial porosity of the nanostructured YSZ layer and the oxidation rate constants of the oxidized systems at 1100°C are presented in Tab. 7.2.

Tab. 7.2 *Initial porosity of nanostructured YSZ layer and oxidation rate constants obtained in PhD thesis and other literature studies*

Coating type	Porosity of YSZ nano [%]	Oxidation exponent, *n*	Oxidation rate constant, *kp*	
			[$m^2 \cdot s^{-1}$]	$\mu m/h^{0.5}$
E1T1	12,87	2	2,18E-17	0,280
E3T1	16,21	2	2,19E-17	0,281
E2T3	20,94	2	2,42E-17	0,295
Keyvani A. et al. 2012	7,3	2	1,22E-17	0,209

Daroonparvar M. et al. 2018	10,5	2	2,01E-17	0,269
Sezavar A. et al. 2019	26	2	2,62E-17	0,307

The results presented in Tab. 7.2 were used as input data in a program written in Matlab to develop a mathematical model describing the interdependence between the initial porosity of the nanostructured YSZ layer in a substrate/TBC coating system and the oxidation rate constant resulting from oxidation at 1100°C. The program starts by inputting the values of the two variables: porosity (expressed in per cent) and oxidation rate constant (expressed in $\mu m/h^{0.5}$) (see Table 7.2). Then, a linear interpolation of the values was performed using the *interp2* instruction and the *pchip* method in Matlab. The curve that passes closest to the experimental points (interpolation curve) plotted in Fig. 7.19 was generated to improve the results. To obtain a function of the oxidation rate constant as a function of porosity "Kp=f(porosity)" the *polyfit* instruction in Matlab was used, based on which a polynomial function of degree 4 was obtained, described by Relation 7.9, which fits the interpolation curve generated in the previous step (Fig. 7.19). To obtain a function of the oxidation rate constant as a function of porosity "Kp=f(porosity)", the Matlab polyfit instruction was used to obtain a polynomial function of degree 4, described by Relation 7.9, which defines the interpolation curve generated in the previous step (Fig. 7.19).

$$F(kp)= -0{,}00000723\ porozitate^4 + 0.00052926\ porozitate^3 - 0.01408424\ porozitate^2 + +0{,}16321359\ porozitate - 0{,}41773066 \quad (7.9)$$

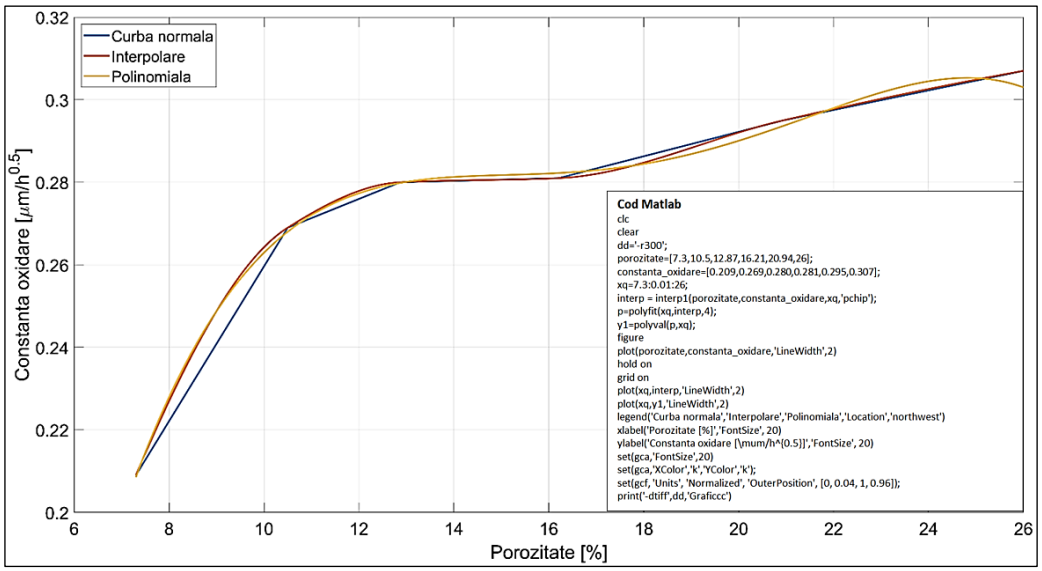

Fig. 7.19 *Graphical representation of interpolation and polynomial functions based on the program written in Matlab*

The mathematical model described by Relation 7.9 has particular practical utility in all phases of the development of thermal spray technology of TBC coating due to the following advantages:

- It gives an accurate prediction of the oxidation behaviour at 1100°C of the substrate/TBC coating system with nanostructured YSZ;
- The oxidation exponent *n* and hence the oxidation rate constant of a coating can be deduced without the need to test it for hundreds of hours at elevated temperatures;

- Can ensure optimal design of components in a substrate/ TBC coating system;
- Mathematically modelled process variables (porosity and oxidation rate constant) are two indicators of TBC coating system performance that can be relatively easily determined;
- By expanding the experimental database and processing it statistically, the mathematical model can be improved/adapted for other temperature ranges or oxidation times, provided that the same technology deposited the coatings.

7.8 Thermal shock testing of substrate/TBC coating systems

The experimental models of substrate/coating TBC systems developed (Fig. 7.20) were tested under laboratory conditions much more severe (thermal shock testing) than the operating conditions in a gas turbine engine. The thermal shock tests were performed using an automated installation for thermal shock, oxidation and corrosion testing of TBC coatings, which was developed in the PhD thesis and for which the patent application no. A 2020 00191 dated 08.04.2020 has been filed and published on 30.10.2020 under no. 134516 A0 (****Buletinul oficial de proprietate industrială, 2020*). The invention will also be presented at the *25th edition of the International Exhibition of Inventions*, INVENTICA 2021, Iasi, Romania.

According to the invention, the stop and start cycles of a stationary or aviation turbine are simulated by performing heating/cooling cycles of two samples tested simultaneously under predefined conditions (heating and cooling temperature, cycle durations), where cooling can be slow or very fast (thermal shock), with or without the addition of corrosive compounds (CMAS compounds or mixed Na_2SO_4 and V_2O_5 compounds), depending on engine specifications, operating conditions etc. In the test installation, these heating-cooling cycles are repeated until the self-detection degradation system registers a decrease in the area of the sample surface covered by 20% compared to the initial state, the limit specified in ISO 13123:2011 (****ISO 13123 2011*).

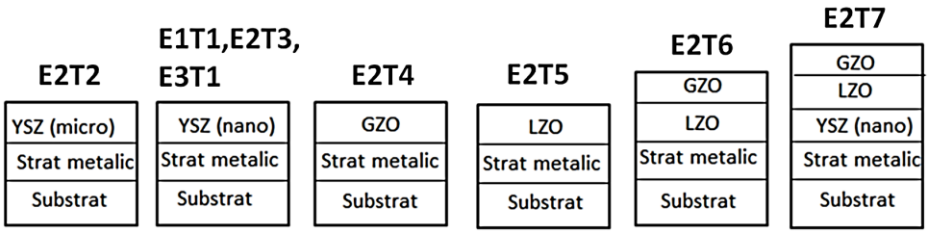

Fig. 7.20 *Experimental models of substrate/ TBC coating systems tested in thermal shock cycles*

In the first stage, the experimental models of substrate/TBC coating systems (Fig. 7.20) were tested under the following conditions:

- Maximum test temperature: 1100°C;
- Minimum cooling temperature: 70°C;
- Sample heating time: 200 sec;
- Holding time at 1100°C: 900 sec;
- Cooling time to 70°C: 195 sec;
- The total duration of one thermal cycle: 22 minutes;
- Test completion criteria: 20% exfoliation of the total coating surface.

Fig. 7.21.a shows the automated thermal shock test installation, and Fig. 7.21.b shows the comparative results for the thermal shock resistance of TBC coatings expressed based on the maximum number of thermal cycles until 20% of the total coating surface has been exfoliated.

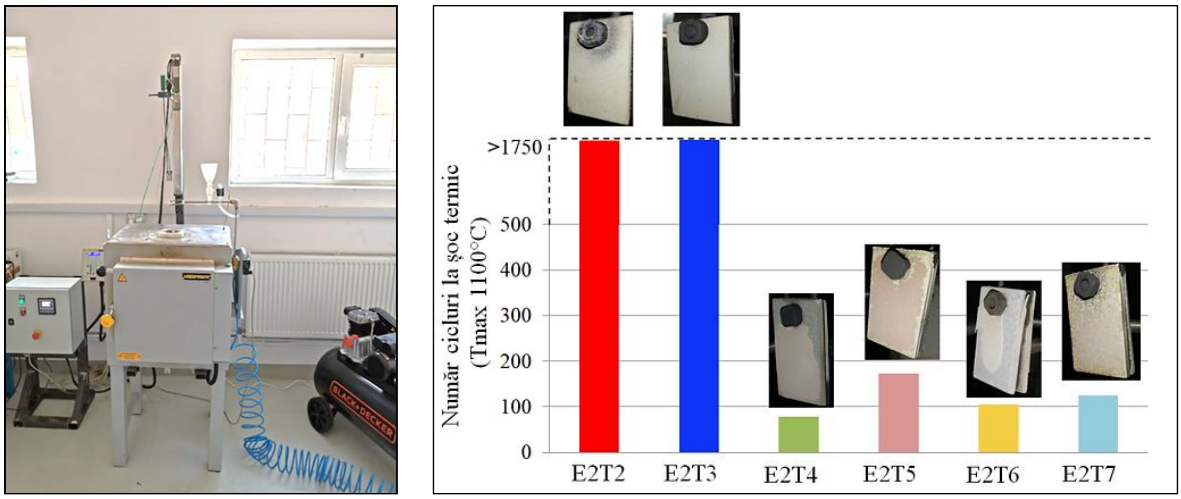

a) *b)*

Fig. 7.21 *Thermal shock testing of developed substrate/TBC coating systems: (a) automated test installation of substrate/TBC coating systems and (b) thermal shock resistance (70-1100°C) of systems (E2T2-E2T7)*

The systems with rare earth Zr oxide as top coats (*E2T4*, *E2T5*, *E2T6* and *E2T7*) exhibited very poor thermal shock resistance (Tmax=1100°C) (maximum 172 cycles - E2T5). This behaviour was predicted in the thermo-structural simulation (see § 6.1), which showed that the highest internal stresses are found in the system with lanthanum and gadolinium zirconate due to differences in the thermal expansion coefficients of the materials composing the system. Mahade S. et al. (2016) proposed a solution, also considered in these experiments, using a YSZ interlayer between the metallic bond coat and the rare earth Zr oxide layers (*E2T7* system). In this case, there was a slight increase of up to 125 cycles. However, even this is insignificant compared to the 1750 cycles (totalling more than 640 hours of testing) that systems with conventional YSZ (*E2T2*) (Fig. 7.22.c) and nanostructured YSZ (*E3T2*) (Fig. 7.22.d) have successfully withstood without cracking, delamination or spallation of the ceramic layers.

a) *b)* *c)* *d)*

Fig. 7.22 *Images during thermal shock cycling tests: (a-b) samples during heating/cooling cycles, (c-d) samples with conventional YSZ and nanostructured YSZ coating after 1750 thermal shock cycles (70-1100°C)*

Based on these preliminary results, the study of thermal shock behaviour has focused on testing under more aggressive conditions experimental models of conventional YSZ and nanostructured YSZ systems, using increasingly higher temperatures (1150°C, 1250°C and 1300°C) and shorter heating/cooling cycle times to amplify the thermal shock effect.

In thermal shock tests with a maximum temperature of 1150°C, the number of cycles when the nanostructured YSZ coating (*E2T3*) degraded was 828, which is about 25% higher than the conventional YSZ system (*E2T2*). The nanostructured YSZ coated system had superior thermal shock resistance to the conventional YSZ coated system for the following two reasons:

- The TGO layer growth is slower in the system with nanostructured YSZ (see § 7.6, Fig. 7.12), inducing lower stresses in the coating layers;
- Nanoparticle agglomerations in the nanostructured YSZ layer reduce the propagation of cracks formed during heating/cooling cycles (Fig. 7.23.a-b). The same effect of the nanoparticle agglomerates was also observed in the fracture toughness tests (see § 7.5.2, Fig 7.8.b).

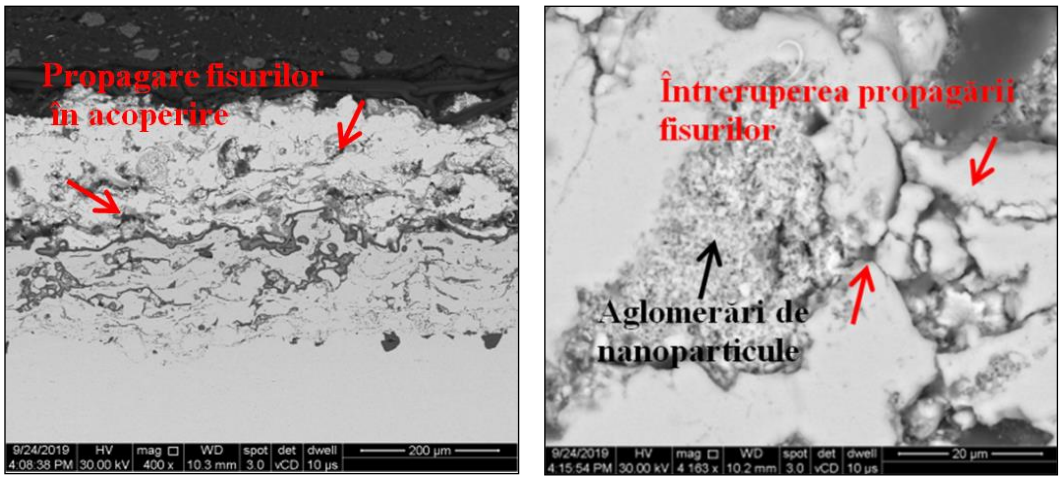

a) *b)*

Fig. 7.23 *SEM images highlighting the crack propagation mode in the nanostructured YSZ (E2T3) layer after 828 cycles at temperatures between 70-1150°C: (a) image acquired in the cross-section of the system and (b) image acquired in the surface of the ceramic layer*

After thermal shock testing at a maximum temperature of 1150°C of the systems with nanostructured YSZ (*E1T1*, *E2T3*, *E3T3*), the following conclusions were obtained:

- The use of a system with nanostructured YSZ (*E2T3*) and two metallic bond coats deposited by high-velocity oxygen-fuel (HVOF) and atmospheric plasma spraying (APS) instead of one bond coat (deposited by APS) can provide an improvement of the thermal shock resistance of the coatings by more than 8%.
- The thermal shock resistance of systems with nanostructured YSZ (*E2T3*) was not influenced by the substrate manufacturing technology (lamination and additive manufacturing) and ranged between 830 cycles (system with conventionally manufactured substrate) and 840 cycles (system with additively manufactured substrate).
- The thermal shock resistance of the system with a high thickness (360 µm) and low porosity (12.87%) of the nanostructured YSZ layer (*E1T1*) was 1337 cycles, which was 60% higher than

that of the system with a low thickness (154 µm) and high porosity (20.94%) of the nanostructured YSZ layer (E3T3).

Additionally, the nanostructured YSZ system (*E1T1*) with the highest thermal shock resistance at 1150°C was tested at maximum temperatures of 1200°C and 1300°C. The thermal shock tests at 1250°C showed a thermal shock resistance of 451 cycles, being more than 60% lower than the same system tested at 1150°C. After testing at a maximum temperature of 1300°C, the thermal shock resistance decreased to 36 cycles, being more than 90% lower than that obtained on the same system tested at thermal shock at a maximum temperature of 1250°C (Fig. 7.24).

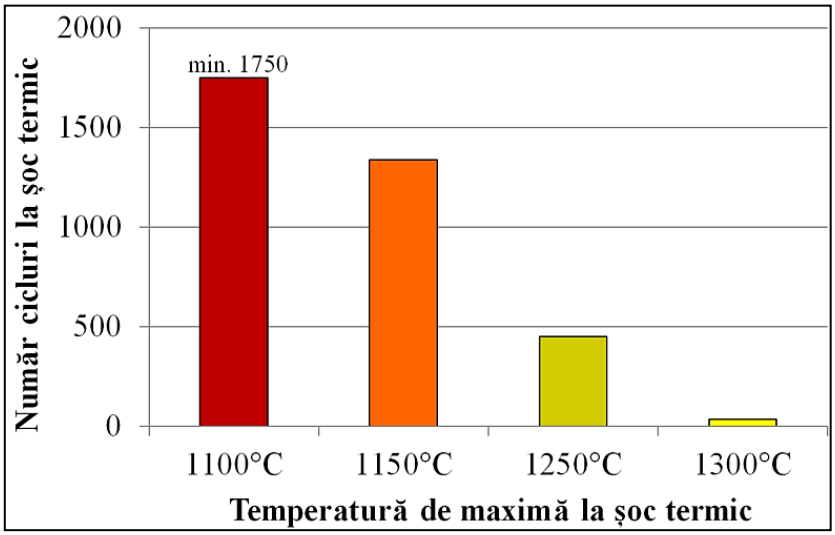

Fig. 7.24 *Thermal shock resistance of nanostructured YSZ (E1T1) systems at maximum temperatures test of 1100°C, 1150°C, 1250°C and 1300°C*

7.9 Thermal spraying of TBC coating on the additive manufactured turbine blade

Based on the experimental results obtained in the high-temperature tests, it was found that the system with nanostructured YSZ E1T1 exhibited the best performance in both long-term cyclic oxidation and thermal shock.

The manufacturing technology of the coating with nanostructured YSZ (E1T1) was further used for the coating of the experimental additively manufactured turbine blade by SLM technology (see § 5.3). The sequence and characteristics of the deposited layers are as follows:

- First metallic bond coat: NiCrAlY alloy deposited with a thickness of 30 µm and roughness of 4 µm, using HVOF technology and the process parameters presented in Tab. 7.3;
- Second metallic bond coat: NiCrAlY alloy deposited with a thickness of 135 µm and roughness of 10 µm, using APS technology and the process parameters presented in Tab. 7.3.
- Top coat: 8% yttria-stabilized nanostructured zirconia (obtained from agglomerations of nanometric sized particles) with a thickness of 360 µm, deposited by thermal spraying using the parameters presented in Tab. 7.3.

***Tab. 7.3** Process parameters used for turbine blade coating*

First metallic bond coat NiCrAlY alloy)		**Second metallic bond coat NiCrAlY) & Ceramic nanostrucured YSZ**		
HVOF spray parameters		Plasma spraying parameters - APS		
Parameters	NiCrAlY	Parameters	NiCrAlY	YSZ nano
Argon (bar)	4.5	Argon (NLPM)	45	40
Hydrogen (bar)	6.0	Hydrogen (NLPM)	6	10.6
Voltage (V)	50	Air jet (bar)	5	5
Amperage (A)	550	Voltage (V)	61	70
Spray distance (mm)	170	Amperage (A)	550	530
Spray angle (˚)	90	Spray distance (mm)	125	100
-	-	Injection nozzle (mm)	8	6
-	-	Spray angle (˚)	90	90
-	-	Spray rate g/min	50	50
-	-	Spray speed (m/min)	75	75
-	-	Spray advance (mm/step)	4	4
-	-	Gun passes	2	2

After that, the additively manufactured blade was fixed in a fixture and coated according to previous specifications. Fig. 7.25.a-d shows images during the coating process of the additively manufactured blade.

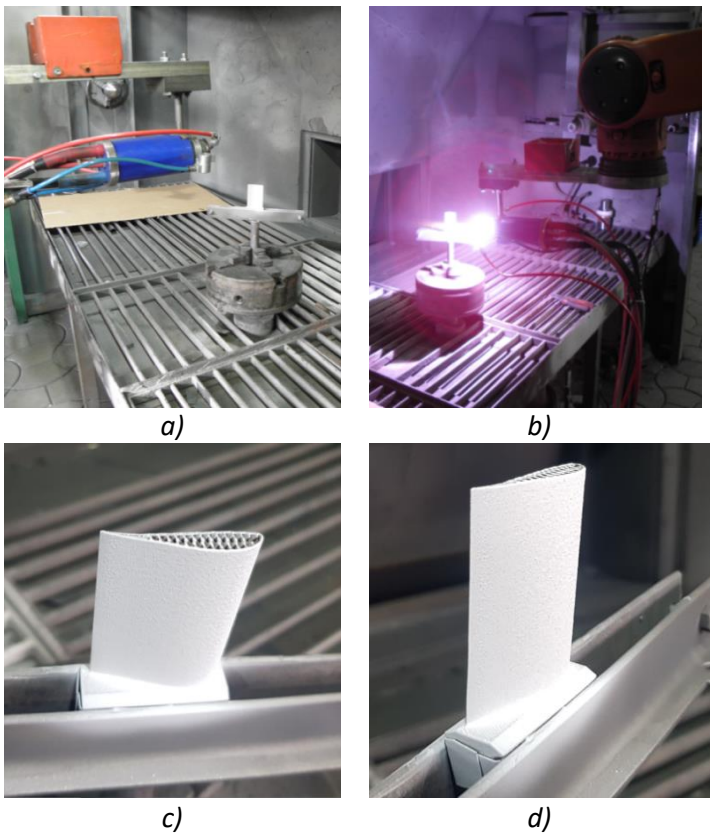

a) *b)*

c) *d)*

***Fig. 7.25** Images during the aerofoil coating process of the additively manufactured turbine blade: (a) metal layer deposition, (b) ceramic layer deposition, and (c-d) TBC coated turbine blade with nanostructured YSZ layer (E1T1)*

Fig. 7.26 shows the main stages in the turbine blade manufacturing process with TBC coating using the SLM technology for the substrate and the thermal spray technology for the TBC coating: I. 3D design of the blade; II. 3D model processing and process parameter selection; III. additive manufacturing of the blade using SLM technology; IV. removal of powder and support structures; V. Sandblasting of blade surfaces; VI. Spraying of TBC coating on the aerofoil surfaces of the blade.

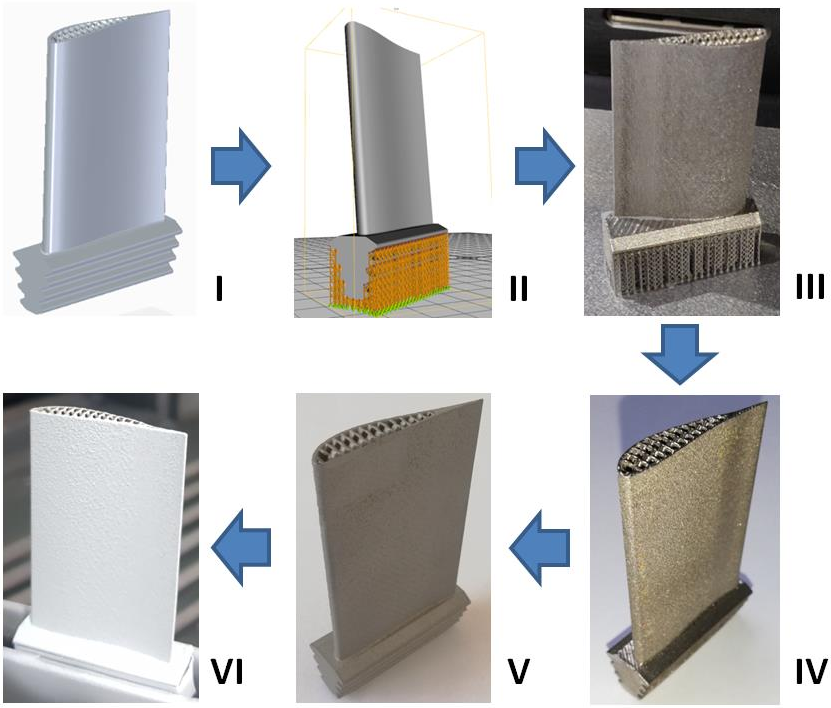

Fig. 7.26 *The stages of the manufacturing process of the experimental model of turbine blade with cooling channels and TBC coating using additive manufacturing and thermal spraying technologies*

Usually, for the additively manufactured parts, extensive research is required on the post-processing operations necessary to meet the technical and operational requirements of the blade: stress-relieving and ageing heat treatment, hot isostatic pressing, surface grinding and finishing, and surface blasting. Additional inspection of geometric and dimensional accuracy and non-destructive testing is required to meet the dimensional and geometric tolerances of turbine blades imposed by aviation standards. Furthermore, in the case of a new product produced by such a technology, extensive research and long-term testing under conditions similar to those in service are required to validate and certify the product. Such research on post-processing and inspection operations that apply to additively manufactured turbine blade, as well as product testing under service conditions, are future research directions.

Based on the research and experimental results obtained in the PhD thesis on the development of additive manufacturing and thermal spraying technologies for increasing the operating performance of complex gas turbine components, it can be concluded that the main objective has been successfully achieved.

Chapter 8. Conclusions, personal contributions and future research directions

8.1 General conclusions

The PhD thesis, entitled, "***Research on the development of innovative manufacturing technologies for increase the performance of complex gasodynamic components***", approached a new topic not thoroughly explored worldwide, of great interest, especially in the aerospace and energy fields, with the main objective of developing innovative manufacturing technology for a complex gasodynamic component blade-type in a gas turbine engine, combining the SLM additive manufacturing technology for the substrate manufacturing with thermal spray technology for the deposition of a thermal barrier coating. The thesis briefly introduces the domains of additive manufacturing and thermal barrier coatings and is structured into eight chapters.

General conclusions drawn from the research are as follows:

- Selective Laser Melting (SLM) is one of the technologies that use the Powder Bed Fusion (PBF) process for manufacturing metal parts and is a promising alternative to conventional technologies for manufacturing components with complex geometries, especially for the energy and aerospace industries, due to the following advantages: freedom design, the manufactured materials have high mechanical performance comparable to conventionally produced materials, the production stages are significantly reduced and manufacturing costs and times are reduced compared to conventional technologies;
- SLM technology has several limitations and disadvantages represented by the structural defects of the manufactured material, anisotropy of mechanical properties, the need of using support structures for the construction of the parts and the need for pre- and post-processing operations for finishing/improving the additively manufactured parts;
- To achieve the maximum potential of SLM technology is necessary to optimise the critical process parameters (current intensity, laser exposure time and layer thickness) and to identify the optimal orientation of the part on the manufacturing platform according to the requirements;
- SLM technology is a viable solution for manufacturing of a turbine blade with improved operating performance, under advantageous conditions, capable of exceeding the performance of a blade produced by conventional technologies;
- The use of Thermal Barrier Coatings (TBC) to protect the complex gasodynamic components contributes to an increase in their capability to operate at elevated temperatures and, consequently, to an increase in the overall performance of the turbine engine;
- TBC coatings with yttria-stabilised zirconia as a top coat (conventional YSZ) provide protection against oxidation and corrosion at elevated temperatures but have a short lifetime relative to the operating life of an engine and are limited to operating temperatures up to 1200°C due to the sintering process and phase transformations of the zirconia;
- The literature study revealed that the most promising materials for replacing the YSZ conventional layer are yttria-stabilised zirconia obtained from nanoparticle agglomerates (nanostructured YSZ), lanthanum and (LZO) and/or gadolinium zirconate (GZO), and the most

successful technology for their deposition is thermal plasma spraying under atmospheric conditions (APS);

- The mechanical properties, microstructural characteristics and fabrication times of the parts are influenced by the critical parameters in the SLM process (exposure time, current intensity and layer thickness) and the building orientation of the part on the manufacturing platform. Therefore, to optimize the process parameters was opted to modify the process parameters independently and not in combination. The primary evaluation criterion was the alloy's mechanical strength.
- By modifying each process parameter on several levels, specimens and samples were manufactured, mechanically tested, and microstructurally analysed in the as-built state based on an experimental design. The most important experimental results are summarised below:
  - The laser exposure time does not significantly influence the mechanical properties but can affect the alloy microstructure and surface quality when it exceeds 40 µs;
  - Increasing the current intensity of the laser beam has a positive impact on the mechanical performance and density of the IN 625 alloy, but also a negative effect in terms of deformations and internal stresses induced in the parts;
  - The thickness of the melt layer strongly influences both the mechanical properties and surface quality of additively manufactured parts and the productivity of the manufacturing process. In general, the mechanical strength of the alloy decreases with increasing layer thickness.
  - The following process parameters have been identified as optimal:
    - Current intensity: 2000 mA;
    - Laser exposure time: 40 µs;
    - Layer thickness: 50 µm;
- IN 625 alloy obtained by SLM technology shows an anisotropy of mechanical properties. The anisotropy is influenced by the orientation of the parts on the manufacturing platform. The orientation of the specimens influences the cooling rates of the alloy (during the solidification process), which define the orientation of the columnar grains. The lowest mechanical performance of additively manufactured IN 625 alloy is obtained when the orientation of the parts is on the Z-axis of the manufacturing platform. However, the experimental results showed that irrespective of the orientation of the specimens on the manufacturing platform (on the X, Y, Z axes and rotated at 45° in the XY plane), after optimisation of the process parameters, it is possible to obtain an IN 625 alloy with a fine microstructure, without defects or deformations and with a mechanical strength higher than the minimum values specified by the standards for this alloy, manufactured additively and conventionally (forging).
- The process parameters identified as optimal based on the mechanical tests and microstructural investigations were used to manufacture support samples (required for deposition, testing and characterization of TBC coatings) and an experimental turbine blade demonstrator with internal cooling channels.
- To identify the optimal building orientation of a turbine blade with cooling channels are required several iterations to determine the minimum angle between two surfaces where the use of

support structures is not necessary, in such a way that the airfoil of the blade or inner cooling channels are not affected, and no significant post-processing operations are required;

- By analysing the temperature distribution and internal stresses using numerical simulation, the most effective TBC coatings can be identified in terms of a temperature drop on the substrate, but also those most susceptible to spallation during high-temperature exposure;
- To validate the results obtained from the numerical simulation, additively and conventionally fabricated IN 625 alloy substrate samples were coated with experimental models of TBC coatings with different coating characteristics and chemical compositions.
- Generally, the substrate/TBC coating systems are tested in long-term cyclic oxidation (minimum 500 hours) and thermal shock cycles at temperatures of minimum 1100°C to simulate (in a more aggressive way) the operating conditions in a gas turbine engine.
- For the validation of a substrate/TBC coating system, comprehensive analyses are required, both in the initial state and after different oxidation times at elevated temperatures, on the mechanical behaviour, microstructure and micro-compositions of the layers, oxidation kinetics, the evolution of the roughness of the metallic bond coat, thickness of the increased oxide layer and porosity of the ceramic layer;
- The substrate/TBC coating systems with nanostructured YSZ are superior to conventional YSZ and especially to the systems with La and/or Ga Zr oxide, both in high-temperature oxidation behaviour and thermal shock resistance.
- Conventional methods and techniques for assessing the porosity of the ceramic layer and metallic bond coat surface roughness of the substrate/TBC coating systems may be inadequate and inaccurate. The development of a quantitative measurement methodology of porosity of the ceramic layer based on SEM image processing can significantly improve the assessment of this characteristic, even for nanopores that conventional methods cannot detect. Furthermore, the development of a methodology for non-contact measurement of surface roughness parameters (Ra, Rz, Rq and Rp) of the metallic bond coat helps to understand better the effects of oxidation on the components in a TBC substrate/coating system, and it can give an accurate long-term prediction of its behaviour at elevated temperatures.
- The development of a mathematical model describing the interdependence between the initial porosity of the nanostructured YSZ layer in a substrate/TBC coating system and its oxidation rate constant has a high practical utility in all stages of TBC coating technology development due to the possibility to provide a pertinent prediction of the service life of a substrate/TBC coating system and to contribute to the optimal development of TBC coatings.
- Manufacturing technology of the substrate (additive or conventional manufacturing) does not significantly influence the high-temperature performance of substrate/TBC coating systems.
- The thermal shock resistance of substrate/TBC coating systems with two metallic bond coats deposited by HVOF and APS thermal spray technologies is superior to the systems with a single metallic bond coat deposited by APS technology. In addition, the porosity and thickness of the nanostructured YSZ layer in a substrate/TBC coating system also have a significant influence on the thermal shock resistance.

- Based on the testing of several models of substrate/TBC coating systems with different layer thicknesses and porosity levels of nanostructured YSZ, the experimental TBC coating model with the highest resistance to oxidation and thermal shock was identified.
- The deposition technology of the best performing experimental TBC coating model was used for coating the experimental additively manufactured turbine blade model. Thus, the main objective of the PhD thesis on the development of innovative technology for the manufacture of a complex gasodynamic component blade-type by combining additive SLM manufacturing technology and thermal spray technology has been achieved.

8.2 Personal contributions

The practical importance of the results obtained in the present PhD thesis is supported by several personal contributions brought in the field of additive manufacturing and thermal spraying for increasing the operating performance of complex gasodynamic components in the gas turbine engine. The main contributions are as follows:

1. A critical review of the literature regarding the state of the art of additive manufacturing and thermal spray technologies used for the manufacture of complex gasodynamic components;
2. Carrying out a study on the impact of increasing operating temperatures on increasing thrust and specific fuel consumption in the F100-220 turbojet-engine used in F16 and F15 military aircraft;
3. Optimisation of the critical process parameters of the SLM technology (current intensity, laser exposure time, and melt thickness) through tests and analyses that mainly targeted the mechanical properties and microstructural characteristics of IN 625 alloy;
4. Highlighting the anisotropy of the mechanical properties of additively fabricated IN 625 alloy based on the mechanical test results and fractographic analyses of specimens manufactured with different orientations on the fabrication platform;
5. Manufacturing by SLM technology of an experimental turbine blade demonstrator with internal cooling channels so that the aerofoil and internal cooling channels of the blade are not affected by the support structures and do not require significant post-processing operations;
6. Numerical simulation modelling in Ansys software of the high-temperature performance of the TBC substrate/coating systems to be developed by analysing the temperature distribution and internal stresses in the layers;
7. Manufacturing of laminated and additively fabricated IN 625 substrate samples on which innovative TBC coatings with one or more top layers consisting of conventional YSZ, nanostructured YSZ with or without Zr oxides with La and/or Gd were deposited, varying certain atmospheric plasma deposition parameters;
8. Analysis of the mechanical properties of substrate/TBC coating systems based on Vickers microhardness tests with different indentation loads;
9. Development of a methodology for non-contact measurement of surface roughness parameters (Ra, Rz, Rq and Rp) of the metallic bond coat in a substrate/TBC coating system (exposed at high-temperature oxidation) using scanning electron microscopy (for capturing SEM images of the bond coat surface in cross-section) and a program developed in Matlab to perform the following

operations: processing of SEM images, determination of the roughness profile, application of correction filters and calculation of roughness parameters;

10. Using the non-contact roughness measurement methodology to analyze the evolution of bond coat surface roughness in substrate/TBC coating systems with conventional YSZ and nanostructured YSZ tested at high-temperature oxidation;
11. Using an innovative method to determine the fracture toughness of ceramic coatings by Vickers microhardness testing and measurement by scanning electron microscopy of the crack length generated around microhardness indentations following the exceeding of the critical indentation load;
12. Development of a methodology for the quantitative assessment of micro- and nano-sized pores in the ceramic layer of a TBC coating by measuring the total area of pores (based on the associated pixels) and relating it to the whole area under investigation, using the binarization techniques and processing of SEM images captured in the cross-section of the coatings;
13. Using the methodology developed for quantitative porosity determination for the analysis of the porosity evolution of conventional YSZ and nanostructured YSZ coatings exposed to oxidation at high temperature;
14. Analysis of the kinetics of the oxidation process of TBC coatings with conventional YSZ and nanostructured YSZ, using TGO layer thickness measurements for finding the actual values of the oxidation exponent *n* and for the calculation of the oxidation rate constants of the investigated systems;
15. Identification of interdependence between the initial porosity of the nanostructured YSZ layer in a substrate/TBC coating system and the oxidation rate constant of the coating that was used for developing an original mathematical model with significant practical utility in all phases of the development of thermal spraying technology for the TBC coatings;
16. Design and develop an automated installation for thermal shock, oxidation and high-temperature corrosion testing of experimental models of substrate/TBC coating systems under similar or more aggressive conditions than in a gas turbine engine. The installation has an integrated auto-detection system for surface degradation of coatings and can automatically perform short (thermal shock) or long (cyclic oxidation) heating/cooling cycles, with or without the addition of corrosive compounds;
17. To patent the invention entitled "Automated installation for thermal shock, oxidation and corrosion testing of thermal barrier coatings", patent application no. A 2020 00191 dated 08.04.2020 was filed, and on 30.10.2020, the patent was published under number 134516 A0. The invention will also be presented at the 25th edition of the International Exhibition of Inventions, INVENTICA 2021, Iasi, Romania.
18. Carrying out thermal shock tests at different temperatures/durations of the substrate/TBC coating systems using the automated installation for thermal shock, oxidation and corrosion testing and comparative analysis of their thermal shock resistance.

8.3 Future research directions

The challenging issue of developing a complex gasodynamic component, using additive manufacturing and thermal spray technologies, under technically and economically more advantageous conditions than conventionally manufactured components, requires a comprehensive research and development activity focusing on several research directions.

The achievement of the activities planned in the future R&D directions can ensure, using additive manufacturing and thermal spraying technologies, the development of the experimental laboratory model and subsequently (after reaching TRL 6), the prototype turbine blade with TBC coatings, by carrying out the following activities:

a) Extending research on post-processing of additively manufactured turbine blades to ensure the quality and compliance (after printing) with the dimensional and geometric tolerances required for blades used in aviation;
b) Analysis of dimensional control of the additively manufactured blade (by conventional and 3D scanning methods) and scaling of the 3D model of the blade to comply with the requirements of an engine specification.
c) Testing of the additively manufactured turbine blade under actual working conditions, using a dedicated stand for turbine engine testing;
d) Researching the behaviour of substrate/ TBC coating systems to combined thermal shock, oxidation and corrosion cycles at high temperatures, using the experimental installation
e) Additive manufacturing of a turbine blade from another alloy (Ti, Al, CoCr or steel) and optimisation of its manufacturing process;
f) Researching the compatibility of the TBC coatings developed in the thesis for other components additively or conventionally manufactured from Ti, Al, CoCr alloys or refractory steels.
g) Analysis of the oxidation kinetics of substrate/coating TBC systems tested at temperatures of 1000°C and 1150°C for durations up to 1000 hours;
h) Increase the technological maturity level of the experimental model of TBC coating with rare earth Zr oxide layer(s) deposited by thermal spraying and/or electron beam physical vapour deposition technologies;

A part of the experimental results obtained in the PhD thesis was disseminated by presenting papers at national and international conferences and publishing articles as a first author and co-author in journals.

A. Presentations at international conferences:

1. **Paraschiv A.**, Matache G., Condruz M.R., Badea T.A., I. Ionica, 8th International Conference on Materials Science and Technologies, November 26-27th, 2020, Bucharest, Romania.
2. **Paraschiv A.**, Matache G., Frigioescu T.-F., Vladut M., Scanning strategy and laser re-melting influence on top surface deformation of additively manufactured IN 625, Oral presentation, 3rd

International Conference on Emerging Technologies in Materials Engineering – EmergeMAT, 29-30 October 2020, Bucharest, Romania;

3. Matache G., **Paraschiv A.**, Condruz M. R., Pambaguian L., Toma A., Puscasu C., Optimization of selective laser melting process parameters for high-density IN625, Oral presentation, Aerospace Europe Conference 2020, 25-28 February 2020, Bordeaux, France;
4. **Paraschiv A.,** Matache G., Condruz M. R., Influence of the layer thickness and scan speed on the microstructure and mechanical properties of SLM Inconel 625, Oral presentation, 11th International Conference on Materials Science and Engineering – BraMat 2019, March 13-16 2019, Brașov, Romania.
5. Matache G., **Paraschiv A.**, R. M. Condruz, Edge and corner effects in selective laser melting of in 625 alloy G. Matache, M. Vladut, Oral presentation, 2ND International Conference on Emerging Technologies in Materials Engineering, 6-8 November 2019, Bucharest, Romania;
6. **Paraschiv A.**, Banu A., Doicin C. and Ionica I., Microstructure and isothermal oxidation behaviour of nanostructured yttria partially stabilized zirconia thermal barrier coatings, Poster section, 11th International Conference on Materials Science and Engineering – BraMat 2019, March 13-16 2019;
7. **Paraschiv A.**, Gheorghe M., Condruz R., Effect of laser scanning speed on microstructure and mechanical properties of selective laser melted Inconel 625**,** Premiul I - Poster section at the 1st International Conference on Emerging Technologies in Materials Engineering EmergeMAT, November 14th- 16h, 2018, Bucharest, Romania.

B. Presentation to be held at an international conference:

Paraschiv A., T. Frigioescu T. A. Badea, Ion Ionica, (2021), Image analysis algorithms for measuring the interfacial roughness in TBCs systems, paper accepted for presentation at the conference Thirteenth Conference of the Euro-American Consortium for Promoting the Application of Mathematics in Technical and Natural Sciences, Albena, Bulgaria, June 24-29.

C. Articles published in journals:

1. **Paraschiv A**., Banu A., Doicin C. and Ionica I., (2020), Isothermal oxidation behavior of plasma-sprayed conventional and nanostructured YSZ thermal barrier coatings, U.P.B. Sci. Bull., Series B, Vol. 82(2), pp. 163-174. ISI indexed article.
2. Banu A., **Paraschiv A.**, Petrescu S., Atkinson I., Anghel E. M., Marcu M., (2020), Isothermal Oxidation Behavior of Novel Al2O3 / NiCrAlY / Ti3Al System at 850°C, Rev. Chim., Vol. 71(5), pp. 106-116, https://doi.org/10.37358/RC.20.5.8118. Revistă ISI (zona gri – Q3), impact factor 1.605;
3. Matache G., **Paraschiv A.** and Condruz M. R., (2020), Tensile Notch Sensitivity of Additively Manufactured IN 625 Superalloy, Materials, Vol. 13(21), pp.1-24, doi:10.3390/ma13214859. Revistă ISI, impact factor 3.057;

4. Matache G., Vladut M., **Paraschiv A.**, Condruz R. M., (2020), Edge and corner effects in selective laser melting of IN 625 alloy, Manufacturing Rev. Vol. 7(8), https://doi.org/10.1051/mfreview/2020008. ISI indexed article;
5. Condruz M. R., Matache G., **Paraschiv A.**, (2020), Characterization of IN 625 recycled metal powder used for selective laser melting, Manufacturing Rev. Vol. 7(5) pp. 1-22, https://doi.org/10.1051/mfreview/2020002. ISI indexed article;
6. Badea T. A., **Paraschiv A**., Condruz M. R., Frigioescu T.-F., Zamfir L. C., Ionica I., (2020), Isothermal oxidation behavior and thermal shock resistance of thermal barrier coatings, Jurnalul Științific TURBO, volume VII(1), pp.65-72.
7. Frigioescu T. F., **Paraschiv A.**, Condruz M. R., Badea T. A., Ionica I., (2020a), Finite element analysis of temperature distribution in plasma-sprayed thermal barrier coatings, Jurnalul Științific TURBO, Vol. VII(1), pp. 101-107.
8. Frigioescu T. F., Condruz M. R., **Paraschiv A.,** Badea T. A., Ionica I., (2020b), System and method design for TBC degradation detection, Jurnalul Științific TURBO, vol. VII(1), pp. 73-78.
9. Condruz M.R., Matache G., **Paraschiv A.**, Badea T., Bădiliță V., (2020), High temperature oxidation behaviour of Selective Laser Melting manufactured IN 625, Vol. 10(5), nr. art.668, Metals 2020, pp.1-19, https://doi.org/10.3390/met10050668. Revistă ISI (Q1), impact factor 1.605;
10. Condruz M. R., Matache G., **Paraschiv A.**, Frigioescu T. F., Badea T., (2020), Microstructural and tensile properties anisotropy of Selective Laser Melting manufactured IN 625, Materials 2020, Vol. 13(21), pp.1-22, doi: 10.3390/ma13214829. Revistă ISI (Q2), impact factor 3.057;
11. Condruz M. R., Matache G., **Paraschiv A.**, (2020), Computational and experimental microstructure characterization of Selective Laser Melted IN 625, Vol. 82(2), pp.213-224, UPB Scientific Bulletin. ISI indexed article;
12. Sobetki A., Mosinoiu L., **Paraschiv A.**, Corban M., Piticescu R. R., Matache G., (2020), Microstructural aspects of the protective ceramic coatings applied on the surfaces of refractory alloys produced by additive manufacturing, Manufacturing Review Vol.7, Nr.33, https://doi.org/10.1051/mfreview/2020031. ISI indexed article.
13. Banu A., Marcu M., Trusca O., **Paraschiv A.**, Anghel E. M., Atkinson I., (2019), Microstructural Characterization of NiCrFeSiBC Coating During Long-Term Isothermal Oxidation at 850°C, J Therm Spray Tech, Vol. 28(6) pp. 1275-1283, doi: 10.1007/s11666-019-00881-1. Impact factor 2.12;
14. **Paraschiv A.**, Matache G., Puscasu C., (2018), The effects of heat treatment on homogenization of CMSX-4 Single-Crystal Ni-Based Superalloy, Transportation Research Procedia Vol. 29, pp. 303–311, https://doi.org/10.1016/j.trpro.2018.02.027. ISI indexed article;
15. **Paraschiv A.**, Matache G., Puscasu C. and Grigorescu M., A correlation between fracture toughness and cohesion strength of molybdenum thermal sprayed coatings, MATEC Web of Conferences Vol. 145, pp. 1-9 (2018), doi: 10.1051/matecconf/201814502007. BDI article;
16. Condruz M. R., Matache G., **Paraschiv A.**, Pușcașu C., (2018), Homogenization Heat Treatment and Segregation Analysis of Equiaxed CMSX-4 Superalloy for Gas Turbine Components Journal of Thermal Analysis and Calorimetry Vol. 134, pp. 443-453**.** Impact factor 1.953;

17. **Paraschiv A.**, Matache G., C.Puscasu, Condruz R., (2017), Non-Contact Roughness Investigation of Ball-Cratered Molybdenum Thermal Spray Coatings, Applied Mechanics and Materials Journal, Vol. 859, pp. 9-14, https://doi.org/10.4028/www.scientific.net/AMM.859.9. BDI article;
18. Matache G., **Paraschiv A.**, Pușcașu C., Condruz M. R., (2017), Simulation Segregaton in CMSX-4 Superalloy: Experiments and Simulation Predictions, Jurnalul Științific TURBO, Vol. IV(1), pp. 11-14;
19. Matache G., **Paraschiv A.**, Puscasu C., (2016), An Investigation of the Thermal Sprayed Molybdenum Coatings Behaviour to Mico-abrasion Wear, Applied Mechanics and Materials, 841, pp. 15-20, https://doi.org/10.4028/www.scientific.net/AMM.841.15. BDI article;
20. Banu A., Marcu M., Petrescu S., Ionescu N. and **Paraschiv A.**, (2016), Effect of niobium alloying level on the oxidation behavior of titanium aluminides at 850°C, International Journal of Minerals, Metallurgy and Materials, 23(1), pp. 1452 – 1457, DOI: 10.1007/s12613-016-1369-y. Impact factor 0.943;
21. Anghel E. M., Marcu M., Banu A., Atkinson I., **Paraschiv A.**, Petrescu S., (2016), Microstructure and oxidation resistance of a NiCrAlY/Al2O3-sprayed coating on Ti-19Al-10Nb-V alloy, Ceramics International, 42(10), pp. 12148–12155; DOI: 10.1016/j.ceramint.2016.04.148. Impact factor 2.758;
22. **Paraschiv A.**, Matache Gh., Puşcaşu C., Evaluation of Fracture Toughness of Molybdenum Thermal Sprayed Coating, Proceeding from the Advanced Materials and Structures - AMS'15, Timisoara, 16 - 17 October 2015;
23. Matache G., Puscasu C., **Paraschiv A.**, Trusca O., (2015), Investigation of some Intrinsic Properties of Thermal Sprayed Molybdenum Coatings for Railway Axle Applications, Applied Mechanics and Materials Vol. 811, pp. 19-23. BDI article;
24. Marcu M., Banu A., Anghel E. M., **Paraschiv A.,** (2015), Corrosion Behavior of a Thermally Oxidized Orto-Titanium Aluminide in Synthetic Seawater Int. J. Electrochem. Vol. 10, pp. 8284 - 8297; Impact factor 1.500;

D. Articles submitted for publication

1. **Paraschiv A.,** T. Frigioescu T. A. Badea, Ion Ionica, (2021), Image analysis algorithms for measuring the interfacial roughness in TBCs systems, the paper is being published in a Proceeding of American Institute of Physics (AIP) (2021).
2. **Paraschiv A.**, Matache G., Condruz M. R., T. Frigioescu, Ionica I., (2020a), The influence of laser defocusing in selective laser melted IN 625, paper submitted for publication (May 2021) in the issue entitled "Design and Application of Additive Manufacturing" of the journal Materials (ISSN 1996-1944, Impact factor 3.057)

E. Article published in the media:

COMOTI revoluţionează industria turbinelor cu gaze pe baza fabricaţiei aditive cu materiale metalice, MARKET WATCH, (2018), Article available at:

http://www.marketwatch.ro/articol/16039/COMOTI_revolutioneaza_industria_turbinelor_cu_gaze_pe_baza_fabricatiei_aditive_cu_materiale_metalice/. Last accessed: 17.05.2019.

The result of the research activity in areas relevant to the PhD thesis can be summarised as follows:

- Total number of articles published in journals: 38 (according to Google Scholar)
- Number of articles published in ISI indexed journals and volumes: 24 (according to ISI Web of Science)
- Citations in journals: 67 (according to Google Scholar)
- Citations in ISI journals: 41 (according to ISI Web of Science)
- h-index: 4
- i10-index: 2
- Scientific research contracts: 19
- Patents: 3

Selective bibliography

1. Anam M. A.,(2018), Microstructure and mechanical properties of selective laser melted superalloy Inconel 625, Electronic Theses and Dissertation, Paper 3029, University of Louisville.
2. Apostolidis A., (2015), Turbine cooling and heat transfer modelling for gas turbine performance simulation, Thesis Cranfield University, School of Engineering.
3. Ban A. M., Aboutaleb L., (2018), Chapter 5, Optimization of Laser-Based Additive Manufacturing, Laser-Based Additive Manufacturing of Metal Parts Modeling, Optimization, and Control of Mechanical Properties, Ed. CRC Press Taylor & Francis Group, Edited by Bian L., Shamsaei N., and Ushe J.M, ISBN 978-1498739986.
4. Baiamonte L., Marra F., Pulci G., Tirillò J., Sarasini F., Bartuli C., Valente T., (2015), High temperature mechanical characterization of plasma-sprayed zirconia–yttria from conventional and nanostructured powders, Surface & Coatings Technology, Vol. 277, pp. 289–298.
5. Banu A., Paraschiv A., Petrescu S., Atkinson I., Anghel E.M., Marcu M., (2020), Isothermal Oxidation Behavior of Novel Al2O3 / NiCrAlY / Ti3Al System at 850°C, Rev. Chim., Vol.71 (5), pp. 106-116.
6. Bose S., DeMasi-Marcin T. J., (1997), Thermal barrier coating experience in gas turbine engines at Pratt & Whitney, Journal of the Thermal Spray Technology Vol.6(1), pp. 99–104.
7. Brandt M., (2016), The role of lasers in additive manufacturing, Introduction in Laser Additive Manufacturing Materials, Design, Technologies and Applications, Edited by Milan Brandt, Woodhead Publishing Series in Electronic and Optical Materials: Number 88 ISBN: 9780081004333.
8. Caiazzo F., Alfieri, Vittorio P., Argenio and Corrado G., (2017), Laser powder-bed fusion of Inconel 718 to manufacture turbine, Int J Adv Manuf Technol Vol. 93, pp. 4023–4031.
9. Cao X. (2004b), Development of New Thermal Barrier Coating Materials for Gas Turbines, University Bochum, Thesis, Centrul de cercetare Jülich.
10. Delgado J., Ciurana J., Rodríguez C.A., (2012), Influence of process parameters on part quality and mechanical properties for DMLS and SLM with iron-based materials, The International Journal of Advanced Manufacturing Technology Vol. 60, pp. 601–610, doi:10.1007/s001.
11. Evans A. G., Clarke D. R., Levi C. G., (2008), The influence of oxides on the performance of advanced gas turbines, J. Eur. Ceram. Soc., Vol.28, pp. 1405-1419.
12. Fauchais P. L., Heberlein J. V. R., Boulos M., (2014), Thermal Spray Fundamentals: From Powder to Part, Springer, ISBN 978-0-387-68991-3.
13. Feuerstein A, Knapp J., Taylor T., Ashary A., Bolcavage A. and Hitchman N., (2007), Technical and Economical Aspects of Current Thermal Barrier Coating Systems for Gas Turbine Engines by Thermal Spray and EBPVD: A Review, JTTEE Vol. 17, Nr. 2, pp 199–213.
14. Girolamo G. D., Brentari A., Serra E., (2016), Some recent findings on the use of SEM-EDS in microstructural characterisation of as-sprayed and thermally aged porous coatings: a short review, AIMS Materials Science, Vol. 3(2), pp. 404-424.

15. Han P., (2017), Additive Design and Manufacturing of Jet Engine Parts, Engineering Vol. 3, pp. 648-652.
16. Hanzl H., Zetek M., Bakša T., Kroupa T., (2015), The Influence of Processing Parameters on the Mechanical Properties of SLM Parts, Procedia Engineering Vol. 100, pp. 1405 – 1413.
17. Jamali H., Mozafarinia R., Razavi R. S., Ahmadi-Pidani R., (2012), Comparison of thermal shock resistances of plasma-sprayed nanostructured and conventional yttria stabilized zirconia thermal barrier coatings, Ceramics International, Vol. 38(8), pp. 6705-6712.
18. Wilson J. M., (2014), Remanufacturing of turbine blades by laser direct deposition with its energy and environmental impact analysis, Journal of Cleaner Production Vol. 80, pp. 170-178.
19. Jackson R. D., Taylor M. P., Evans H. E., X.-H. Li, (2011), Oxidation Study of an EB-PVD MCrAlY Thermal Barrier Coating System, Oxid. Met., Vol. 76, pp. 259–271.
20. Kempen K., Yasa E., Thijs L., Kruth J.P., Humbeeck J. V., (2011), Microstructure and mechanical properties of selective laser melted 18Ni-300 steel, Physics Procedia, Vol. 12, pp. 255-263.
21. Keyvani A., Saremi M., Heydarzadeh Sohi, Valefi Z., (2012), A comparison on thermomechanical properties of plasma-sprayed conventional and nanostructured YSZ TBC coatings in thermal cycling, Journal of Alloys and Compounds Vol. 541, pp. 488-494.
22. Khaimovich A. I., Kokareva V. V., Smelov V. G., Agapovichev A. V., Sotov A. V., (2019), Development of an Additive Manufacturing Quality System for Gas Turbine Engine Part Production, Engineering Reality Magazin, Vol. 9, pp.64-68.
23. Khoda B., (2017), Chapter 2 Computer-Aided Design of Additive Manufacturing Components, Laser-Based Additive Manufacturing of Metal Parts Modeling, Optimization, and Control of Mechanical Properties, CRC Press Taylor, Edited by L. Bian, N.Shamsaei, and J. M. Usher, ISBN 9781315151441.
24. Kokini K., Takeuchi Y.R., Choules B. D., (1996), Surface Thermal Cracking of Thermal Barrier Coatings Owing to Stress Relaxation: Zirconia vs Mullfite, Surf. Coat. Technol, Vol. 82, pp. 77-82.
25. Kruth J.-P., Badrossamay M., Yasa E., Deckers J., Thijs L., Van HumbeeckPart J., (2010), Material properties in selective laser melting of metals, 16th International Symposium on Electromachining (ISEM XVI), Shanghai, China.
26. Leary M., (2017), Chapter 4, Surface roughness optimisation for selective laser melting (SLM): accommodating relevant. Edited by Milan Brandt, Woodhead Publishing Series in Electronic and Optical Materials: Nr. 88, pp. 99-118.
27. Lee A. S., Singh R., Probert S., (2009), Modelling of the Performance of a F100-PW229 Equivalent Engine under Sea-level Static Conditions, 45th AIAA/ASME/SAE/ASEE Joint Propulsion Conference & Exhibit 2 - 5 August, Denver, Colorado.
28. Lima R. S., Marple B. R., (2008), Nanostructured YSZ thermal barrier coatings engineered to counteract sintering effects, Materials Science and Engineering, Vol. 485, pp. 182–193.
29. Liu B., Li B.-Q., Li Z., (2019), Selective laser remelting of an additive layer manufacturing process on AlSi10Mg, Results in Physics Vol.12, pp.982–988.
30. Li. R., Zhang M.,(2015), Overview on Thermal Barrier Coatings Application and Development, International Journal of Research in Engineering and Science Vol. 3(7), pp. 33-35.

31. Liu B., Wang J. Y., Zhou Y. C., Liao T., Li F. Z., (2007), Theoretical elastic stiffness, structure stability and thermal conductivity of La2Zr2O7 pyrochlore, Acta Mater Vol. 55, pp. 2949-2957.
32. Liu R., Wang Z., Sparks T., Liou F., Newkirk J., (2017), Chapter 13 - Aerospace applications of laser additive manufacturing in Laser additive manufacturing, Woodhead Publishing, pp. 351-371.
33. Liu X., Wang T., Li C., Zheng Z., Lin Q., (2016), Microstructural evolution and growth kinetics of thermally grown oxides in plasma sprayed thermal barrier coatings, Progress in Natural Science: Materials International, Vol. 26, pp. 103–111.
34. Magerramova L., Turichin G., Nozhnitsky T.A., Klimova-Korsmik O., Vasiliev B., Volkov M. and Salnikov A., (2018), Peculiarities of additive technologies application in the production of gas turbine engine parts, Journal of Physics Conference Series, Vol. 1109(1):012051, pp.1-9.
35. Mahade S., Li R., Curry N., Bjorklund S., Markocsan N., Nyl P., (2016), Isothermal Oxidation Behavior of Gd2Zr2O7/YSZ Multilayered Thermal Barrier Coatings, Int. J. Appl. Ceram. Technol Vol.13(3), pp. 443-450.
36. Muktinutalapati N. R., (2011), Materials for Gas Turbines – An Overview, Advances in Gas Turbine Technology, Dr Ernesto Benini (Ed.), pp. 293-314
37. Nickels L., (2015), AM and aerospace: An ideal combination. Met. Powder Rep., Vol. 70, pp. 300–303.
38. Odhiambo J. G., Li W., Zhao Y. and Li C., (2019), Porosity and Its Significance in Plasma-Sprayed Coatings Coatings, Vol.9 (460), pp. 1-19.
39. Pan W., Phillpot S. R., Wan C., Chernatynskiy A., Qu Z., (2012), Low thermal conductivity oxides, MRS Bulletin Vol. 37, pp. 917-922.
40. Pankotai F., Rawlins F., (2018), Gas turbine AM components for new production and repair opportunities, AM WG's meeting, ETN.
41. Paraschiv A., Matache G., Puscasu C., Grigorescu M., (2018c), A correlation between fracture toughness and cohesion strength of molybdenum thermal sprayed coatings. MATEC Web of Conferences, Vol.145, pp. 1-9, doi: 10.1051/matecconf/201814502007
42. Paraschiv A., Matache G., Puscasu C., Condruz R., (2016), Non-Contact Roughness Investigation of Ball-Cratered Molybdenum Thermal Spray Coatings, Applied Mechanics and Materials 859, pp. 9-14.
43. Paraschiv A., Matache G., Puscasu, C. (2018a), The effect of heat treatment on the homogenization of CMSX-4 Single-Crystal Ni-Based Superalloy, Transportation Research Procedia, Vol.29, pp. 303–311, https://doi.org/10.1016/j.trpro.2018.02.027.
44. Paraschiv A., Banu A., C. Doicin and I. Ionica, (2020c), Isothermal oxidation behavior of plasma-sprayed conventional and nanostructured YSZ thermal barrier coatings, U.P.B. Sci. Bull., Series B, Vol. 82(2), pp. 163-174.
45. Petrat T., Graf B., Gumenyuk A. and Rethmeier M., (2016), Laser metal deposition as repair technology for a gas turbine burner made of Inconel 718," Physics Procedia, Vol. 83, pp. 761 – 768.

46. Pimin Z., (2018), Oxidation behaviour of MCrAlX coatings: effect of surface treatment and an Al-activity based life criterion, Thesis, Linköping Studies in Science and Technology Licentiate Thesis No. 1799.
47. Rohnke M., Janek J., Kilner J. A., Chater R. A., (2004), Surface oxygen exchange between yttria stabilised zirconia and a low-temperature oxygen rf-plasma, Solid State Ionics 166 (1/2), pp. 89-102.
48. Salvati E., Lunt A., Ying S., Sui T., Zhang H., Heason C., Baxter G., Korsunsky A. M., (2017), Reconstruction of Residual Strains in an Additively Manufactured and Shot Peened Nickel Superalloy Compressor Blade, Computer Methods in Applied Mechanics, Vol. 320, pp.335-351.
49. Shaikh A. S., (2018), Development of a γ' Precipitation Hardening Ni-Base Superalloy for Additive Manufacturing,". Thesis for: Master of Science in Materials Engineering, Department of Industrial and Materials Science, Gothenburg, Sweden 2018.
50. Song B., Dong S., Coddet P., Liao H., Coddet C. (2014), Fabrication of NiCr alloy parts by selective laser melting: columnar microstructure and anisotropic mechanical behavior. Materials & Design, Vol.53(Nr.1-7), doi:10.1016/j.matdes.2013.07.010.
51. Smelov V. G., Sotov A. and Agapovichev A., (2016), Research on the possibility of restoring blades while repairing gas turbines engines parts by selective laser melting, International Seminar on Interdisciplinary Problems in Additive Technologies. IOP Conference Series Materials Science and Engineering 140(1):012019.
52. Sufiiarov V. A., Popovich A. A., Borisov E. V., Polozov I. A., Masaylo D. V., Orlov A. V., (2017), The effect of layer thickness at selective laser melting, Procedia Engineering, Vol. 174, pp. 126 – 134.
53. Sun J., Zhang L., Zhao D., (2010), Microstructure and thermal cycling behavior of nanostructured yttria partially stabilized zirconia (YSZ) thermal barrier coatings, Journal of Rare Earths, Vol. 28, pp. 198-201.
54. Thijs L., Montero Sistiaga M. L., Wauthle R., Xie Q., Kruth J.-P. and Humbeeck J. V., (2013), Strong morphological and crystallographic texture and resulting yield strength anisotropy in selective laser melted tantalum, Acta Mater., Vol.61, Nr.12, pp. 4657-4668.
55. Ulmeanu M., Doicin C., (2018), Dezvoltarea produselor fabricate aditiv. Editura Bren, ISBN 978-606-610-219-3, 427 pagini.
56. Vassen R., Cao X., Tietz F., Basu D., and Stöver D., (2000), Zirconates as new materials for thermal barrier coatings, Journal of the American Ceramic Society, Vol. 83, pp. 2023-2028.
57. Vaßen R., Jarligo M.O., Steinke T., Mack D.E., Stöver D., (2010), Overview on advanced thermal barrier coatings, Surface and Coatings Technology, Vol. 205, pp. 938-942.
58. Wang L., Zhong X.H., Zhao Y.X., Tao S.Y., Zhang W., Wang Y., Sun X.G., (2014), Journal of Asian Ceramic Societies, Vol. 2(2), pp. 102–116.
59. Wang W. Q., Sha C. K., Sun D. Q., Gu X. Y., (2006), Microstructural feature, thermal shock resistance and isothermal oxidation resistance of nanostructured zirconia coating, Materials Science and Engineering: A, Vol. 424, pp.1–5.

60. Wu J., Guo H., Zhou L., Wang L., Gong S., (2010), Microstructure and Thermal Properties of Plasma Sprayed Thermal Barrier Coatings from Nanostructured YSZ, Journal of Thermal Spray Technology, Vol.19(6), pp. 1186–1194.
61. Yu Z., Dharmasena K. P., Hass D. D., Wadley H. N. G., (2006), Vapor deposition of platinum alloyed nickel aluminide coatings, Surface & Coatings Technology , Vol. 201, pp. 2326-2334.
62. Zhang L. C., Klemm D., Eckert J., Hao Y.L., Sercombe T. B., (2011), Manufacture by selective laser melting and mechanical behavior of a biomedical Ti–24Nb–4Zr–8Sn alloy, Scripta Materialia, Vol. 65, pp. 21–24.
63. ***Community Research ***Navrotsky V., (2018), State of the Art Additive Manufacturing in the gas turbine components (ETN meeting's presentation).
64. ***Dassault Systemes, (2018), Available at: https://make.3dexperience.3ds.com/processes/sheet-lamination, Last accessed 04.02.2018.
65. ***ETN Additive Manufacturing Working Group, (2019), Best practices for defects detection in additively manufactured components in the energy sector, ETN Global, pp.1-50.
66. ***González D. S., Álvarez, A. G., (2018), AM Manufacturing Feasibility Study & Technology Demonstration, EDA AM State of the Art & Strategic Report, Available at: https://eda.europa.eu/docs/default-source/projects/eda-am-study-and-strategic-report_v6.pdf. Last accessed 03.08.2020.
67. ***National Aeronautics and Space Administration, Available at: https://data.nasa.gov/dataset/TBC-with-High-Temperature-Phase-Stability-for-Low-/by4i-n86t, Last accessed 04.05.2020.
68. ***Siemens 3D Printed Gas Turbine Blades, (2016), Available at: http://www.powerworldanalysis.com/siemens-achieves-breakthrough-3d-printed-gas-turbine-blades/, Last accessed 04.11.2019.
69. ***SIEMENS Gas Turbine Blades, (2018), Available at: https://pubs.spe.org/en/ogf/ogf-article-detail/?art=3882, Last accessed 04.09.2018.
70. ***Siemens 3D Printed Gas Turbine Blades, (2016), Available at: http://www.powerworldanalysis.com/siemens-achieves-breakthrough-3d-printed-gas-turbine-blades/, Last accessed 04.11.2019.
71. ***Standard ISO/ASTM DIS 52900, (2018), Additive manufacturing – General principles – Terminology.
72. ***TURBOCAM International, (2018), Available at: http://www.turbocam.com/direct-metal-laser-sintering-dmls, Last accessed 12.11.2019.